confirmed in at least three independent karyotypes, whereas other abnormalities were found in at least two karyotypes.[2] Complex karyotypes were defined by the presence of more than two independent karyotypes with at least three unrelated aberrations according to the previous studies.[16,17] Clinical records were reviewed retrospectively at each hospital according to the above criteria and after fully anonymized, the cases who met the criteria were reported according to an indicated form with regard to patients' age, sex, diagnosis (French–American–British (FAB)), date of diagnosis, cytogenetics (G-banding), histories of chemo-radiotherapies, cellularity and blast counts of bone marrow, complete peripheral blood counts at diagnosis, presence or absence of leukemic transformation, and date and cause of death. The list of the collaborating hospitals is the Hematology unit of Akita University Hospital and Dokkyo University Hospital, Honma Hospital, Jichi Medical School Hospital, National Kyushu Cancer Center, Nishio Municipal Hospital, Saitama Medical School Hospital, Showa University Fujigaoka Hospital, Tokyo Medical School Hospital, the Hospital of Tokyo Women's Medical University and the University of Tokyo Hospital. The diagnosis and sub-classification of MDS and AML at each collaborating hospital were made according to the FAB criteria.[18] Mutation study was performed for 20 cases each with der(1;7)(q10;p10) and −7/7q-, for which genomic DNA from bone marrow was available. Another 20 MDS cases showing normal karyotypes were also subjected to the mutation analysis, according to the approval from the ethical committee, University of Tokyo (Approval No. 948-1).

Statistical analysis

The statistical difference in each clinical feature between der(1;7)(q10;p10) and other −7/7q cases was tested by 2×2 contingency tables using the Fischer's exact test or the Student's *t*-test. Overall survival was estimated using the Kaplan–Meier method and the statistic significance was calculated using log-rank tests. After possible association with overall survival was individually tested for a number of variables, including age, bone marrow blasts, peripheral blood counts, chromosomal abnormalities and history of anticancer therapies, proportional hazard modeling was used for identifying the independent risk factors that influence overall survival, where those factors that showed potential significance in the univariate tests with $P<0.10$ were subjected to the multivariate analysis using backward stepwise selection of covariates. All *P*-values were two-sided and *P*-values of 0.05 or <0.05 were considered statistically significant.

Mutation analysis

Mutation status of the *runx1/AML1 and N-ras* genes was tested on aforementioned 60 cases. Exons 3, 4, 5, 6, 7b and 8 of the *runx1* gene and exons 1 and 2 of the *N-ras* gene were amplified from genomic DNA by polymerase chain reaction (PCR) as described previously.[19,20] Sequencing was performed using an ABI Prism 3100 Genetic Analyzer with the same primers as used in PCR amplification.

Literary review of der(1;7)(q10;p10) cases

Reported cases of der(1;7)(q10;p10) were retrieved from the Mitelman Database of Chromosome Aberrations in Cancer 2006[21] according to the following karyotypic descriptions: der(1;7)(q10;p10); der(1)t(1;7)(p11;p11); +t(1;7)(p11;p11),−7; der(1;7)(p10;q10); and dic(1;7)(p11;q11).

Results

Patients' characteristics

In total, 123 cases, including 22 AML, 98 MDS and 3 MPD, were analyzed. The demographic features of these 123 cases are summarized in Table 1. Seventy-seven cases were der(1;7)(q10;p10), which contain 20 cases reported previously.[22,23] The other 46 cases had −7/7q- other than der(1;7)(q10;p10). Strong male predominance was evident in both groups, especially in der(1;7)(q10;p10). The cases having der(1;7)(q10;p10) accounted for 2.3% (10 cases) of 427 cases who were diagnosed as having AML or MDS at the University of Tokyo Hospital. −7/7q- was found in 38 cases among the 427 cases, of which 22 and 16 cases were diagnosed as having MDS and AML, respectively. Both showed a high median age of the disease onset but it was higher in der(1;7)(q10;p10) than for −7/7q- ($P=0.0027$). In our series, 32.9% of der(1;7)(q10;p10) and 25.0% of −7/7q- cases had one or more prior histories of chemotherapies and/or radiotherapies for some malignancies. In both groups, more cases are diagnosed as MDS than as AML. Increased eosinophil counts in der(1;7)(q10;p10) have been underscored in some literatures,[13,24,25] but in our series it was not so conspicuous and only six der(1;7)(q10;p10) and one −7/7q- cases had prominent eosinophilia ($>450/\mu l$).

Cytogenetic features

Karyotypic analysis revealed a number of cytogenetic features which contrast der(1;7)(q10;p10) to other 7q- abnormalities (Supplementary Table 1 and 2). der(1;7)(q10;p10) was always present at the time of clinical diagnosis and even when multiple subclones exist, it involves all the abnormal karyotypes. In 45 (58.4%) cases, it appeared as a sole chromosomal abnormality during the observation periods. The remaining 32 cases had additional chromosomal abnormalities, but they were limited in number and mostly consisted of trisomy 8 (18 cases) and/or loss of 20q (10 cases). In contrast, −7/7q- appeared as the solitary abnormality was less common (28.3%) and it was more typically accompanied by other frequently complex abnormalities, where 24 of the 46 −7/7q- cases showed more than four additional unrelated chromosomal abnormalities. Indeed, the mean number of additional abnormalities was significantly higher in the −7/7q cases than in der(1;7)(q10;p10) cases ($P<0.0001$) (Table 1). Moreover, in some cases, it appeared only in partial karyotypes (−7/7q- cases 5, 6, 22, 23, 28, 31 and 35) and evolved during the course of the diseases. 5q- was the most common abnormality that was found in association with −7/7q- (23/46), whereas trisomy 8 and 20q- were very rare in this group.

der(1;7)(q10;p10) in MDS

Since the majority of cases in this study were diagnosed as MDS (FAB classification[18]), it is of interest to focus the analysis on those cases having MDS (Table 2). In fact, clinical features were considerably different between both cytogenetic groups in MDS. According to the FAB classification, der(1;7)(q10;p10) cases were more likely to be classified into RA ($P=0.0002$), whereas RAEB/RAEB-t were the leading diagnosis in the −7/7q- group ($P=0.0003$). Similarly, der(1;7)(q10;p10) cases were more frequently classified into favorable risk groups than −7/7q- cases ($P<0.0001$) in the International Prognostic Scoring System (IPSS),[16] where more Int-1-risk cases ($P<0.0001$) and less high-risk cases ($P<0.0001$) were diagnosed in der(1;7)(q10;p10) than in −7/7q- cases. In accordance with this was that bone marrow

Table 1 Clinical characteristics of patients with der(1;7) and −7/7q-

	der(1;7)	*−7/7q-*	P-*value***	*der(1;7) Mittelman**	P-*value****
Number of patients	77	46		125	
Male/female	68/9	36/10	0.1963	74/51	<0.0001
Median age	67 (17–88)	58 (21–78)	0.0027	58 (7–86)	<0.0001
Positive prior history of chemoradiotherapy	25/76 (32.9%)	10/40 (25.0%)	0.4045		
Time to diagnosis (month)	105 (8–224)	76 (15–135)	0.1057		
Diagnosis					
MDS	64	34	0.2512	77	0.0015
AML	10	12	0.0888	33	0.0329
M0	2	1		2	
M1	1	2		3	
M2	3	4		4	
M4	2	1		8	
M5	0	0		0	
M6	0	3		0	
M7				3	
AML, NS	1	0		13	
MLL(Ph+)	1	1		0	
MPD	3	0		13	
Additional chromosomal abnormalities					
Total	32 (41.6%)	33 (71.7%)	0.0015	45 (36.0%)	0.4581
Trisomy 8	18	1	0.0014	25	0.5983
Trisomy 21	2	1		8	0.3235
Trisomy 9	1	0		4	0.6513
del(20q)	10	4	0.5666	2	0.0014
−5/5q-	1	23	<0.0001	3	
Number of additional chromosomal abnormalities					
1	23	7	0.0837	29	0.3223
2	7	2	0.4935	7	0.3975
3	1	4	0.0645	4	0.6513
⩾4	2	24	<0.0001	5	0.7108
PB					
WBC ($\times 10^3/\mu l$)	3.0 (0.8–39)	3.35 (0.3–56.9)	0.1072		
Hb (g/dl)	9.4 (2.8–13.8)	7.9 (3.8–15.0)	0.0150		
PLT ($\times 10^4/\mu l$)	8.1 (1.3–87)	5.75 (0.6–70.8)	0.2542		
Eosino ($/\mu l$)	45 (0–16932)	0 (0–740)	0.2720		
$>450/\mu l$	6	1			
BM					
Hypercellular	16/69	17/42	0.0585		
Normocellular	31/69	16/42	0.5544		
Hypocellular	22/69	9/42	0.2795		

Abbreviations: AML, acute myeloid leukemia; BM, bone marrow; Eosino, Median eosinophil count; Hb, median hemoglobin level; MDS, myelodysplastic syndrome; MLL, mixed lineage leukemia; MPD, myeloproliferative disorders; NS, not specified; PB, peripheral blood; PLT, median platelet count; WBC, median white blood cell count.
*Non-Asian cases from the Mitelman database of chromosome aberrations in cancer.
***P*-values are calculated between der(1;7)(q10;p10) and −7/7q- cases in the current series or ****P*-values between ours and Mittelman's der(1;7)(q10;p10) cases.

blast counts were significantly lower in der(1;7)(q10;p10) cases than in −7/7q- cases ($P<0.0001$). Also anemia tended to be less severe at the time of diagnosis in der(1;7)(q10;p10) than in −7/7q- cases ($P=0.0075$). More than half cases in both groups were transformed into AML but der(1;7)(q10;p10) cases showed significantly slower progression to AML than −7/7q- cases ($P=0.0043$). Accordingly more patients tend to have been treated by chemotherapy in −7/7q- group than in der(1;7)(q10;p10) group ($P=0.049$). In total, 57 deaths had occurred during the observation period. Infection was the most common cause of deaths in the der(1;7)(q10;p10) group without leukemic transformation (11 of 16 informative cases), whereas MDS patients were more frequently transformed to AML before death in the −7/7q- group (14/22 in −7/7q- vs 14/35 in der(1;7)(q10;p10)).

Allogeneic stem cell transplantation was performed in two der(1;7)(q10;p10) and three −7/7q- cases. The two der(1;7)(q10;p10) cases survived 1184 and 1508 days after transplantation, whereas two of the three −7/7q- cases succumbed to death within a year due to relapse or complication of the transplantation. Among non-transplanted cases, the der(1;7)(q10;p10) group showed significantly better clinical outcome than other −7/7q- cases, although there was significant heterogeneity with regard to therapies. The median overall survivals were 710 and 272 days in der(1;7)(q10;p10) and other −7/7q- cases, respectively ($P<0.0001$) (Figure 1). In univariate analyses of all MDS cases, >10% blast counts ($P=0.0006$) and cytopenia in two or more lineages ($P=0.0189$) were also extracted as significant risk factors. However, after the backward step-wise liner regressions, only −7/7q- karyotypes ($P<0.0001$)

and 60 years or more ages ($P=0.0148$) were extracted as independently significant risk factors, indicating der(1;7)(q10;p10) and −7/7q- karyotypes define separate risk groups (Table 3).

Table 2 Clinical characteristics of MDS patients with der(1;7) and −7/7q-

	der(1;7)	*−7/7q-*	P-*value*
MDS	64	34	
Male/female	57/7	27/7	0.2310
Median age	67 (17–88)	60 (22–78)	0.0974
De novo MDS	44	20	0.9999
Positive prior history of chemoradiotherapy	20	8	
WBC ($\times 10^3/\mu l$)	3.0 (0.8–34.0)	2.4 (0.3–24.0)	0.7043
Hb (g/dl)	9.0 (2.8–13.7)	7.8 (3.8–12.1)	0.0075
PLT ($\times 10^4/\mu l$)	8.0 (1.3–87)	8.1 (0.8–71)	0.9293
BM blast (%)	3.0 (0–14.0)	7.2 (0–29)	<0.0001
Trisomy 8	17	1	0.0048
del(20q)	10	4	0.7651
−5/5q-	0	20	<0.0001
Diagnosis			
RA	39	7	0.0002
RAEB	9	12	0.0203
RAEBt	6	9	0.0379
CMMoL	4	3	0.6908
MDS, NS	6	3	0.9999
IPSS			
High	5	14	0.0002
Int-2	29	17	0.6766
Int-1	31	2	<0.0001
Therapy			
Chemotherapy	11/59	10/24	0.0491
Allo HSCT	2	3	
Transformation to AML (%)	33 (51.6%)	22 (64.7%)	0.2853
Median time to transform (month)	12.0	4.23	0.0043
Median overall survival (month)	23.7	9.07	<0.0001
Death (infection)	39 (18)	22 (8)	

Abbreviations: AML, acute myeloid leukemia; BM, bone marrow; CMMoL, chronic myelomonocytic leukemia; Hb, median hemoglobin level; HSCT, hematopoietic stem cell transplantation; IPSS, international prognostic scoring system; MDS, myelodysplastic syndrome; NS, not specified; PLT, median platelet count; RA, refractory anemia; RAEB, refractory anemia with excess of blasts; RAEBt, RAEB in transformation; WBC, median white blood cell count.

Mutation of runx1 *and* N-ras *genes*

Since high rates of *runx1* mutations have recently been reported in association with −7/7q- cases,[19,26,27] we examined mutation status of *runx1* in 20 der(1;7)(q10;p10) as well as 20 −7/7q- cases together with additional 20 MDS cases without cytogenetic abnormalities. More *runx1* mutations were found in der(1;7)(q10;p10), but it was not significant (7 der(1;7)(q10;p10), 2 −7/7q- and two other cases with normal karyotypes). There were no correlations between mutations and specific FAB subtypes, blast counts or over all survivals, although the sample numbers being too small. *N-ras* mutaions were found in one der(1;7)(q10;p10) cases (at codon 12), two −7/7q- cases (at codon 12) and two normal karyotypes (at codons 12 and 13), which are comparable to the rates reported previously in MDS.[20,28,29]

Literary review of 125 der(1;7)(q10;p10) cases reported previously in the literatures

In total, 164 entries were retrieved from the Mitelman database as having der(1;7)(q10;p10), of which 39 Asian cases were excluded from the further analyses to prevent duplicated retrievals and to explore the ethnic difference in the clinical and cytogenetic pictures of this translocation (Table 1). They had almost similar demographic and cytogenetic features to the current series, but still showed marked difference in several respects. Compared with Asian cases, the male preponderance

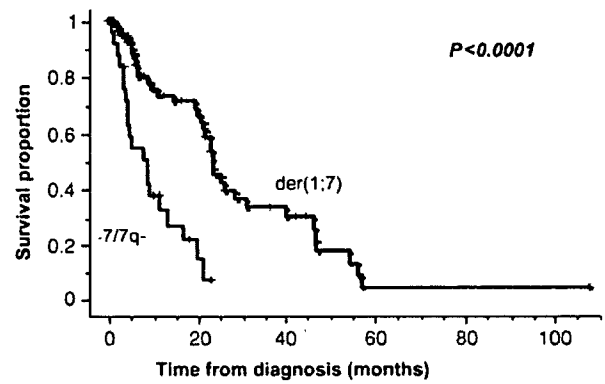

Figure 1 Comparison of survival between der(1;7)(q10;p10) and other −7/7q- cases in MDS. Kaplan–Meier curves of overall survival in MDS cases are compared between der(1;7)(q10;p10) and other −7/7q-. *P*-values in log rank tests are shown.

Table 3 Factors on overall survival

	Univariate		*Multivariate*	
	P-*value*	*HR (95% CI)*	P-*value*	*HR (95% CI)*
MDS cases				
der(1;7) vs −7/7q-	<0.0001	4.240 (2.202–8.164)[a]	<0.0001	4.787 (2.455–9.333)[a]
Age >60	0.0655	1.724 (0.959–3.096)	0.0148	2.088 (1.155–3.774)
Cycytopenia[b] 2/3	0.0189	1.984 (1.107–3.546)		
BM blast >10%	0.0006	2.810 (1.518–5.205)		
Additional cytogenetic changes	0.1598	1.470 (0.856–2.526)		
Secondary MDS	0.1872	1.473 (0.836–2.470)		

Abbreviations: BM, bone marrow; CI, cumulative interval; HR, hazard ratio; MDS, myelodysplastic syndrome.
[a]Hazard ratio of −7/7q- to der(1;7) group.
[b]Found in more than two lineages as defined by neutrophil count <1800/μl, platelets <10,000/μl, Hb <10 g/dl.

is not prominent and diagnosis of MDS and del(20q) abnormalities seem to be less common in the Western cases.

Discussion

We retrospectively analyzed 77 der(1;7)(q10;p10) cases in order to disclose clinical and cytogenetic features of this translocation, focusing on comparison to other −7/7q- cases, since loss of 7q material is a cardinal consequence of this unbalanced translocation as well as gain of 1q material. In spite of the common 7q loss, we found significant differences between both cytogenetic groups in terms of hematological pictures, clinical outcome and cytogenetic characteristics.

der(1;7)(q10;p10) cases tend to be presented with milder anemia, lower blast counts, thus more RA diagnosis, and to show slower progression to AML and have significantly better clinical outcome than other −7/7q- cases. The cytogenetic profiles exhibit a more striking contrast between both groups. der(1;7)(q10;p10) appears as the sole chromosomal abnormality in more than half cases and if not, the additional abnormalities are limited in number and variation, consisting mostly of trisomy 8 and loss of 20q, although the latter has not been described in the Western literatures.[14] In contrast, −7/7q- as the sole abnormality is less common in adult cases but more likely to coexist with other frequently complex abnormalities of partial karyotypes.[4] Common additional abnormalities in −7/7q- cases include −5/5q-, which predicts grave clinical outcomes among −7/7q- group[30] but is rarely found in der(1;7)(q10;p10) cases.

Comparison with der(1;7)(q10;p10) cases reported from the Western countries mostly confirmed the results from our series, but also disclosed a marked contrast between both series. Extreme male predisposition and the common 20q abnormality in our series may indicate that genetic or ethnic background play an important role in the pathogenesis of der(1;7)(q10;p10) positive neoplasms. In our series only two of nine female patients with der(1;7)(q10;p10) are *de novo* cases.

In the past studies, involving relatively small numbers of patients, reported very poor prognosis for this translocation, typically showing less than 1 year of median survival.[3,14,15] However, in the current study including 64 der(1;7)(q10;p10) cases, it appears to have better clinical outcome than reported previously, where the survival curve is roughly overlapped with that of the Int-2 IPSS category with a median survival of 23 months for der(1;7)(q10;p10) cases, which was significantly longer than 9 months of −7/7q-positive MDS cases. This may be explained by the fact that −7/7q- cases showed higher bone marrow blast counts and lower hemoglobin concentration than der(1;7)(q10;p10) cases, which were extracted as significant risk factors in univariate analyses (Table 3). Unexpectedly, however, in multivariate analysis using backward stepwise selection of covariates, only the −7/7q- karyotypes and 60 years or more ages were selected as independent risk factors. Indeed, when the effects of blast counts and cytopenia were adjusted by a proportional hazard model, difference in karyotypes still remains to be significant ($P=0.0034$). These observations suggest that der(1;7)(q10;p10) defines a separate prognostic group that shows significantly better clinical outcome than −7/7q- cases and also indicate a possibility that the der(1;7)(q10;p10) may be more appropriately assigned to an intermediate rather than high-risk karyotype in the IPSS[16] or GCEGCH[17] scoring system for better prediction of prognosis. Unfortunately, however, we were not able to test the latter possibility using our series due to a small number of the cases.

With regard to the pathogenetic role of der(1;7)(q10;p10), no specific molecular targets have been identified for this translocation. Since their breakpoints are distributed widely within the large (~0.5–3 Mb) alphoid cluster regions on the centromeres of chromosome 1 and chromosome 7,[10] no specific gene target at the breakpoints is likely to be involved in the recombination event, but loss of 7q and/or gain of 1q should play a role in the pathogenesis of this translocation. In this point of views, it may be worth mentioning that gains of 1q material are also among recurrent chromosomal abnormalities in MDS.[6,31] Of particular note is that similar 'dicentric' translocations are found in MDS and most frequently involve chromosome 1, resulting in trisomy 1q.[15]

On the other hand, it is still open to questions whether additional genetic hits are required to develop der(1;7)(q10;p10)-positive MDS. According to the cytogenetic profiles of der(1;7)(q10;p10) and −7/7q- cases, different pathogenetic models might be postulated in both cytogenetic groups. der(1;7)(q10;p10) represents a relatively early genetic event and a few additional genetic insults, including +8 and/or 20q-, could be involved in the neoplastic evolution. On the other hand, −7/7q- is likely to be shared by more heterogeneous subgroups and could be a later genetic event during neoplastic process which shows discrete cytogenetic profiles from those involved in der(1;7)(q10;p10). *Runx1* and *N-ras* genes seem to be among common targets of both cytogenetic groups. Especially, a relatively high incidence of *runx*1 mutations (7/20) in our der(1;7)(q10;p10) series should be further confirmed, considering a possible link between runx1 mutations and 7q loss.[19,26]

Conclusion

der(1;7)(q10;p10) defines a unique clinicopathological entity of myeloid neoplasm having a distinct cytogenetic profile and clinical picture. In our study on heterogeneous MDS patients, their clinical outcome is not as bad as reported previously, but still poor with 23 months of median survival, which argues for importance of stem cell transplantation as a potentially curative treatment, and also for development of novel therapeutic approaches.

Acknowledgements

We are grateful to the late Professor Hisamaru Hirai, who initially promoted and encouraged this work. We also thank Dr Masaaki Takatoku of Jichi Medical School and Dr Hiroshi Harada of Showa University Fujigaoka Hospital, Dr Yukihiro Arai of Dokkyo University, Dr Akira Matsuda and Dr Motohiro Misumi of Saitama Medical School, Dr Yuta Koyama of Honma Hospital, Dr Ikuo Miura of Akita University, Dr Hideaki Mizoguchi of Tokyo Women's Medical University and Dr Takuhei Murase of Nishio Municipal Hospital for providing case reports. This work was supported by Research on Measures for Intractable Diseases, Health and Labor Sciences Research Grants, Ministry of Health, Labor and Welfare and by Research on Health Sciences focusing on Drug Innovation, The Japan Health Sciences Foundation.

References

1 Willem P, Pinto M, Bernstein R. Translocation t(1;7) revisited. Report of three further cases and review. *Cancer Genet Cytogenet* 1988; **36**: 45–54.

2 Shaffer L, Tommerup NE. *An International System for Human Cytogenetic Nomenclature (2005).* Karger: Basel, Switzerland, 2005.
3 Horiike S, Taniwaki M, Misawa S, Nishigaki H, Okuda T, Yokota S *et al.* The unbalanced 1;7 translocation in *de novo* myelodysplastic syndrome and its clinical implication. *Cancer* 1990; **65**: 1350–1354.
4 Mauritzson N, Albin M, Rylander L, Billstrom R, Ahlgren T, Mikoczy Z *et al.* Pooled analysis of clinical and cytogenetic features in treatment-related and *de novo* adult acute myeloid leukemia and myelodysplastic syndromes based on a consecutive series of 761 patients analyzed 1976–1993 and on 5098 unselected cases reported in the literature 1974–2001. *Leukemia* 2002; **16**: 2366–2378.
5 Sandberg AA, Morgan R, Hecht BK, Hecht F. Translocation (1;7)(p11;p11): a new myeloproliferative hematologic entity. *Cancer Genet Cytogenet* 1985; **18**: 199–206.
6 Lee DS, Kim SH, Seo EJ, Park CJ, Chi HS, Ko EK *et al.* Predominance of trisomy 1q in myelodysplastic syndromes in Korea: is there an ethnic difference? A 3-year multi-center study. *Cancer Genet Cytogenet* 2002; **132**: 97–101.
7 Toyama K, Ohyashiki K, Yoshida Y, Abe T, Asano S, Hirai H *et al.* Clinical implications of chromosomal abnormalities in 401 patients with myelodysplastic syndromes: a multicentric study in Japan. *Leukemia* 1993; **7**: 499–508.
8 Mertens F, Johansson B, Heim S, Kristoffersson U, Mitelman F. Karyotypic patterns in chronic myeloproliferative disorders: report on 74 cases and review of the literature. *Leukemia* 1991; **5**: 214–220.
9 Reilly JT, Snowden JA, Spearing RL, Fitzgerald PM, Jones N, Watmore A *et al.* Cytogenetic abnormalities and their prognostic significance in idiopathic myelofibrosis: a study of 106 cases. *Br J Haematol* 1997; **98**: 96–102.
10 Wang L, Ogawa S, Hangaishi A, Qiao Y, Hosoya N, Nanya Y *et al.* Molecular characterization of the recurrent unbalanced translocation der(1;7)(q10;p10). *Blood* 2003; **102**: 2597–2604.
11 Scheres JM, Hustinx TW, Geraedts JP, Leeksma CH, Meltzer PS. Translocation 1;7 in hematologic disorders: a brief review of 22 cases. *Cancer Genet Cytogenet* 1985; **18**: 207–213.
12 Morrison-DeLap SJ, Kuffel DG, Dewald GW, Letendre L. Unbalanced 1;7 translocation and therapy-induced hematologic disorders: a possible relationship. *Am J Hematol* 1986; **21**: 39–47.
13 Imai Y, Yasuhara S, Hanafusa N, Ohsaka A, Enokihara H, Tomizuka H *et al.* Clonal involvement of eosinophils in therapy-related myelodysplastic syndrome with eosinophilia, translocation t(1;7) and lung cancer. *Br J Haematol* 1996; **95**: 710–714.
14 Pedersen B. Survival of patients with t(1;7)(p11;p11). Report of two cases and review of the literature. *Cancer Genet Cytogenet* 1992; **60**: 53–59.
15 Pedersen B, Norgaard JM, Pedersen BB, Clausen N, Rasmussen IH, Thorling K. Many unbalanced translocations show duplication of a translocation participant. Clinical and cytogenetic implications in myeloid hematologic malignancies. *Am J Hematol* 2000; **64**: 161–169.
16 Greenberg P, Cox C, LeBeau MM, Fenaux P, Morel P, Sanz G *et al.* International scoring system for evaluating prognosis in myelodysplastic syndromes. *Blood* 1997; **89**: 2079–2088.
17 Sole F, Luno E, Sanzo C, Espinet B, Sanz GF, Cervera J *et al.* Identification of novel cytogenetic markers with prognostic significance in a series of 968 patients with primary myelodysplastic syndromes. *Haematologica* 2005; **90**: 1168–1178.
18 Bennett JM, Catovsky D, Daniel MT, Flandrin G, Galton DA, Gralnick HR *et al.* Proposals for the classification of the myelodysplastic syndromes. *Br J Haematol* 1982; **51**: 189–199.
19 Christiansen DH, Andersen MK, Pedersen-Bjergaard J. Mutations of AML1 are common in therapy-related myelodysplasia following therapy with alkylating agents and are significantly associated with deletion or loss of chromosome arm 7q and with subsequent leukemic transformation. *Blood* 2004; **104**: 1474–1481.
20 Plata E, Viniou N, Abazis D, Konstantopoulos K, Troungos C, Vaiopoulos G *et al.* Cytogenetic analysis and RAS mutations in primary myelodysplastic syndromes. *Cancer Genet Cytogenet* 1999; **111**: 124–129.
21 Mitelman F, Johansson B, Martens FE. Mitelman database of chromosome aberrations in cancer. In: http://cgap.nci.nih.gov/Chromosomes/Mitelman.
22 Hsiao HH, Ito Y, Sashida G, Ohyashiki JH, Ohyashiki K. *De novo* appearance of der(1;7)(q10;p10) is associated with leukemic transformation and unfavorable prognosis in essential thrombocythemia. *Leuk Res* 2005; **29**: 1247–1252.
23 Hsiao HH, Sashida G, Ito Y, Kodama A, Fukutake K, Ohyashiki JH *et al.* Additional cytogenetic changes and previous genotoxic exposure predict unfavorable prognosis in myelodysplastic syndromes and acute myeloid leukemia with der(1;7)(q10;p10). *Cancer Genet Cytogenet* 2006; **165**: 161–166.
24 Forrest DL, Horsman DE, Jensen CL, Berry BR, Dalal BI, Barnett MJ *et al.* Myelodysplastic syndrome with hypereosinophilia and a nonrandom chromosomal abnormality dic(1;7): confirmation of eosinophil clonal involvement by fluorescence *in situ* hybridization. *Cancer Genet Cytogenet* 1998; **107**: 65–68.
25 Kim SH, Suh C, Choi SJ, Kim JG, Lee JH, Kim SB *et al.* Myelodysplastic syndrome that progressed to acute myelomonocytic leukemia with eosinophilia showing peculiar chromosomal abnormality: a case report. *J Korean Med Sci* 1999; **14**: 448–450.
26 Niimi H, Harada H, Harada Y, Ding Y, Imagawa J, Inaba T *et al.* Hyperactivation of the RAS signaling pathway in myelodysplastic syndrome with AML1/RUNX1 point mutations. *Leukemia* 2006; **20**: 635–644.
27 Pedersen-Bjergaard J, Christiansen DH, Desta F, Andersen MK. Alternative genetic pathways and cooperating genetic abnormalities in the pathogenesis of therapy-related myelodysplasia and acute myeloid leukemia. *Leukemia* 2006; **20**: 1943–1949.
28 Padua RA, West RR. Oncogene mutation and prognosis in the myelodysplastic syndromes. *Br J Haematol* 2000; **111**: 873–874.
29 Christiansen DH, Andersen MK, Desta F, Pedersen-Bjergaard J. Mutations of genes in the receptor tyrosine kinase (RTK)/RAS-BRAF signal transduction pathway in therapy-related myelodysplasia and acute myeloid leukemia. *Leukemia* 2005; **19**: 2232–2240.
30 Smith SM, Le Beau MM, Huo D, Karrison T, Sobecks RM, Anastasi J *et al.* Clinical-cytogenetic associations in 306 patients with therapy-related myelodysplasia and myeloid leukemia: the University of Chicago series. *Blood* 2003; **102**: 43–52.
31 Sole F, Espinet B, Sanz GF, Cervera J, Calasanz MJ, Luno E *et al.* Incidence, characterization and prognostic significance of chromosomal abnormalities in 640 patients with primary myelodysplastic syndromes. Grupo Cooperativo Espanol de Citogenetica Hematologica. *Br J Haematol* 2000; **108**: 346–356.

Supplementary Information accompanies the paper on the Leukemia website (http://www.nature.com/leu)

MOLECULAR AND CELLULAR BIOLOGY, Dec. 2007, p. 8190–8204 Vol. 27, No. 23
0270-7306/07/$08.00+0 doi:10.1128/MCB.00661-07

Extracellular Signal-Regulated Kinase/Mitogen-Activated Protein Kinase Regulates Actin Organization and Cell Motility by Phosphorylating the Actin Cross-Linking Protein EPLIN▽†

Mei-Ying Han,[1,2] Hidetaka Kosako,[1]* Toshiki Watanabe,[2] and Seisuke Hattori[1,3]

Division of Cellular Proteomics (BML), The Institute of Medical Science,[1] and Department of Medical Genome Sciences, Graduate School of Frontier Sciences,[2] The University of Tokyo, 4-6-1 Shirokanedai, Minato-ku, Tokyo 108-8639, Japan, and Department of Biochemistry, School of Pharmaceutical Sciences, Kitasato University, 5-9-1 Shirokane, Minato-ku, Tokyo 108-8641, Japan[3]

Received 16 April 2007/Returned for modification 11 June 2007/Accepted 7 September 2007

Extracellular signal-regulated kinase (ERK) is important for various cellular processes, including cell migration. However, the detailed molecular mechanism by which ERK promotes cell motility remains elusive. Here we characterize epithelial protein lost in neoplasm (EPLIN), an F-actin cross-linking protein, as a novel substrate for ERK. ERK phosphorylates Ser360, Ser602, and Ser692 on EPLIN in vitro and in intact cells. Phosphorylation of the C-terminal region of EPLIN reduces its affinity for actin filaments. EPLIN colocalizes with actin stress fibers in quiescent cells, and stimulation with platelet-derived growth factor (PDGF) induces stress fiber disassembly and relocalization of EPLIN to peripheral and dorsal ruffles, wherein phosphorylation of Ser360 and Ser602 is observed. Phosphorylation of these two residues is also evident during wound healing at the leading edge of migrating cells. Moreover, expression of a non-ERK-phosphorylatable mutant, but not wild-type EPLIN, prevents PDGF-induced stress fiber disassembly and membrane ruffling and also inhibits wound healing and PDGF-induced cell migration. We propose that ERK-mediated phosphorylation of EPLIN contributes to actin filament reorganization and enhanced cell motility.

Extracellular signal-regulated kinase (ERK), a member of the mitogen-activated protein kinase (MAPK) family, plays pivotal roles in diverse cellular events, such as proliferation, differentiation, migration, growth, and survival (4, 18, 30, 44). Activation of ERK occurs in response to growth factor stimulation through the Ras-Raf-MEK pathway, and activated ERK translocates from the cytoplasm to the nucleus, where it phosphorylates several protein kinases, nuclear transcription factors, and other proteins (12, 17, 30). In addition to its role in the nucleus, recent data show that ERK is involved as an essential component in the migration of cells from many different organisms (9, 16, 21, 38). Certain substrates, such as myosin light chain kinase (25), focal adhesion kinase (14), paxillin (19), actopaxin (5), calpain (10), and vinexin (24), are known to function in ERK-mediated cell migration (13).

Cell migration requires dynamic reorganization of the actin cytoskeleton (31). Composite extracellular stimuli, including growth factors and cell-matrix adhesions, trigger signals for cell motility, which are then transduced by diverse intracellular components, such as the MAPK family (13, 39), protein kinase B/Akt (36), tyrosine kinases (6), and Rho family small GTPases (8, 34). During dynamic remodeling of the actin system for cell migration, a number of actin cross-linking/bundling proteins are crucial (1, 37, 40, 46). In addition, actin bundles and cross-linked networks play key roles in the generation of tension and flexibility in the actin cytoskeleton (2, 33). Thus, ERK might mediate cell migration via phosphorylating some actin cross-linking/bundling proteins.

Epithelial protein lost in neoplasm (EPLIN) was originally identified as the product of a gene that is transcriptionally down-regulated or lost in a number of human epithelial tumor cells, including oral, prostate, and breast cancer cell lines (3, 22). EPLIN is expressed from a single gene as two isoforms, α and β, the latter of which has an extra N-terminal sequence of 160 amino acids. Both EPLINα and -β contain a centrally located LIM domain that may mediate self-dimerization and N- and C-terminal actin-binding sites flanking the LIM domain (23). EPLIN cross-links and bundles actin filaments, thereby stabilizing actin stress fibers. Furthermore, EPLIN inhibits Arp2/3 complex-mediated branching nucleation of actin filaments. Thus, EPLIN controls actin filament dynamics by stabilizing actin filament networks (23). It is therefore assumed that the loss of EPLIN expression in cancer cells is involved in the enhanced motility of these cells.

Recently, we identified EPLIN as a candidate substrate for ERK by a proteomic approach using two-dimensional difference gel electrophoresis (2D-DIGE) combined with phosphoprotein enrichment. In this study, we show that ERK phosphorylates EPLIN in vitro and in vivo. Phosphorylation of the C-terminal region of EPLIN inhibits its actin-binding activity. Stimulation with platelet-derived growth factor (PDGF) induces stress fiber disassembly and localization of phosphorylated EPLIN to peripheral and dorsal ruffles. Furthermore, expression of a non-ERK-phosphorylatable mutant of EPLIN

* Corresponding author. Mailing address: Division of Cellular Proteomics (BML), The Institute of Medical Science, The University of Tokyo, 4-6-1 Shirokanedai, Minato-ku, Tokyo 108-8639, Japan. Phone and fax: 81-3-6409-2073. E-mail: kosako@ims.u-tokyo.ac.jp.

† Supplemental material for this article may be found at http://mcb.asm.org/.

▽ Published ahead of print on 17 September 2007.

prevents PDGF-induced membrane ruffling as well as cell migration. These results suggest that phosphorylation of EPLIN by ERK leads to reorganization of actin filaments and stimulation of cell motility.

MATERIALS AND METHODS

Cell culture and transfection. ΔB-Raf:ER cells (NIH 3T3 cells expressing the B-Raf kinase domain fused to the estrogen receptor ligand binding domain) (32) were cultured in Dulbecco's modified Eagle's medium (DMEM) without phenol red (Invitrogen, Carlsbad, CA) but containing 10% fetal bovine serum (FBS). NIH 3T3 cells were cultured in DMEM containing 10% calf serum (CS). 293T and HeLa cells were cultured in DMEM containing 10% FBS. Primary calvarial osteoblasts were isolated from 1-day-old Jc1:ICR mice by five sequential digestions (for 10 min each) with 0.1% collagenase and 0.2% dispase. The cells from the last four digestions were grown in α-minimum essential medium (Invitrogen) containing 10% FBS. Transfections were performed by using Lipofectamine 2000 (Invitrogen) for 293T and ΔB-Raf:ER cells and Lipofectamine LTX (Invitrogen) for NIH 3T3 and osteoblastic cells, according to the manufacturer's instructions.

Plasmids and protein expression. The DNA fragments encoding mouse EPLINα (161-753), EPLINβ (1-753), EPLIN-N (161-387), and EPLIN-C (440-753) were amplified by PCR and cloned into pCMV-Tag3-Myc (Stratagene, La Jolla, CA), pCMV-Tag2-Flag (Stratagene), or pGEX-4T-3 vector (GE Healthcare, Buckinghamshire, United Kingdom). For expression of enhanced green fluorescent protein (EGFP)-fused EPLINα in mammalian cells, the DNA fragment encoding EGFP was amplified by PCR and cloned into the C-terminal coding region of pCMV-Tag3-Myc-EPLINα. Point mutations were introduced using a QuikChange site-directed mutagenesis kit (Stratagene) according to the manufacturer's instructions.

Antibodies and reagents. A rabbit polyclonal antibody (PAb) against mouse EPLIN was generated against glutathione *S*-transferase (GST)-fused full-length EPLINα expressed in *Escherichia coli* BL21-CodonPlus (DE3)-RIPL (Stratagene) and was affinity purified with immobilized EPLINα, from which the GST moiety was removed by thrombin digestion. Anti-phosphorylated-EPLIN antibodies were raised by immunizing rabbits with keyhole limpet hemocyanin-conjugated synthetic phosphopeptides corresponding to 11-amino-acid sequences of EPLINα and were purified from antiserum as the bound fraction of a phosphopeptide-conjugated SulfoLink column (Pierce, Rockford, IL) and the unbound fraction of a non-phosphopeptide-conjugated column. The following antibodies were also used: anti-Myc mouse monoclonal antibody (MAb) 9E10, anti-Myc rabbit PAb A-14, anti-ERK1 rabbit PAb K-23 (Santa Cruz Biotechnology, Santa Cruz, CA), anti-p-ERK mouse MAb E10, anti-p-RSK (Thr573) rabbit PAb (Cell Signaling Technology, Danvers, MA), antiactin mouse MAb (Chemicon, Temecula, CA), anti-Flag mouse MAb M2 (Sigma, St. Louis, MO), anti-EPLIN rabbit PAb BL1141 (Bethyl, Montgomery, TX), anti-GFP rabbit PAb (Invitrogen), and antihemagglutinin (anti-HA) rat MAb 3F10 (Roche, Basel, Switzerland). PDGF and 4-hydroxy-tamoxifen (4-HT) were obtained from Sigma. U0126 was purchased from Promega (Madison, WI).

Phosphatase treatment. Myc-EPLINβ was transfected into ΔB-Raf:ER cells. Cells were then treated with 4-HT for 2 h, and cell lysates were immunoprecipitated with an anti-Myc (9E10) antibody. Immunoprecipitates were resuspended in a reaction buffer containing 4 units of calf intestinal alkaline phosphatase (CIAP; Takara, Shiga, Japan) and incubated at 37°C for 60 min. The reaction was stopped by adding Laemmli's sample buffer and boiling the samples. Proteins were separated by sodium dodecyl sulfate-polyacrylamide gel electrophoresis (SDS-PAGE) and subjected to immunoblotting with an anti-Myc (A-14) antibody.

RNAi and rescue assays. EPLIN small interfering RNA (siRNA) and siCONTROL nontargeting siRNA 1 were obtained from Dharmacon (Lafayette, CO). The sequences of siRNA duplexes that target mouse EPLIN are as follows: sense, 5′-GGACGAAUCUACUGUAAGCUU-3′; and antisense, 5′-GCUUACAGUAGAUUCGUCCUU-3′. ERK1 and ERK2 Stealth siRNA duplexes were obtained from Invitrogen. The sequences of mouse ERK1 siRNAs are as follows: sense, 5′-GGAAGCCAUGAGAGAUGUUU ACAUU-3′; and antisense, 5′-AAUGUAAACAUCUCUCAUGGCUUCC-3′. The sequences of mouse ERK2 siRNAs are as follows: sense, 5′-GGCU AAAGUAUAUCCAUUCAGCUAA-3′; and antisense, 5′-UUAGCUGAAU GGAUAUACUUUAGCC-3′. These siRNA duplexes were transfected into NIH 3T3 or primary osteoblastic cells by using DharmaFECT 1 reagent (Dharmacon); and cells were cultured for 72 h. For rescue assays, we constructed an RNA interference (RNAi)-refractory EPLINα cDNA (EPLINαr) and EPLINα(S360/602/692A) cDNA [EPLINαr(S360/602/692A)]. Three silent mutations were introduced into the mouse EPLINα and EPLINα(S360/602/692A) cDNAs, changing the nucleotide sequence at positions 817 to 825 of EPLINα/EPLINα(S360/602/692A) to CG CATATAT.

In vitro kinase assay. Phosphorylation of recombinant GST-EPLINα, GST–EPLIN-N, GST–EPLIN-C, and their Ala substitutes by ERK was performed by incubation of 50 ng of recombinant active ERK2 (New England Biolabs, Beverly, MA) with 3.0 μg each of GST-EPLINα, -N, -C, and their mutants and 50 μM [γ-^{32}P]ATP (2.5 μCi; GE Healthcare) in 30 μl of a kinase buffer (50 mM Tris-HCl, pH 7.5, 15 mM $MgCl_2$, 1 mM EGTA, and 2 mM dithiothreitol [DTT]) for 20 min at 30°C. The reaction was stopped by adding Laemmli's sample buffer and boiling the samples. Half of the sample was subjected to 10% SDS-PAGE, and the phosphorylation reaction was visualized by autoradiography.

LC-tandem mass spectrometry (LC-MS/MS) analysis. GST-EPLINα phosphorylated by ERK in vitro was separated by SDS-PAGE. In-gel digestion was performed using sequencing-grade trypsin (Promega) or endoproteinase Glu-C (Roche). The resulting peptides were separated by C_{18} reversed-phase high-pressure liquid chromatography (LC), and each peptide was analyzed with a matrix-assisted laser desorption ionization–time-of-flight tandem mass spectrometer (model 4700 proteomics analyzer; Applied Biosystems, Foster City, CA). Detected masses and peptide sequences were subjected to database searches with the Mascot search engine (Matrix Science, London, United Kingdom).

Actin cosedimentation assays. Binding of EPLIN to F-actin was tested in a cosedimentation assay as described previously (23). Briefly, rabbit muscle G-actin (Cytoskeleton, Denver, CO) and GST–EPLIN-C or GST–EPLIN-C(S602/692A) were separately precleared by centrifugation at 100,000 × *g* for 30 min at 4°C. G-actin (2.5 μM) was polymerized in 5 mM Tris-HCl, pH 7.5, 100 mM KCl, 2 mM $MgCl_2$, 0.2 mM ATP, and 0.5 mM DTT at room temperature for 30 min. Fifty microliters of F-actin was then incubated with 10 μl of ERK-phosphorylated or nonphosphorylated GST–EPLIN-C or GST–EPLIN-C(S602/692A) for 30 min at 4°C. After being centrifuged at 100,000 × *g* for 30 min at 4°C, the supernatant and pellet were separated and analyzed by SDS-PAGE and Coomassie brilliant blue (CBB) staining.

Immunoprecipitation. Cells were lysed with immunoprecipitation buffer (20 mM Tris-HCl, pH 7.5, 150 mM NaCl, 10 mM NaF, 25 mM β-glycerophosphate, 2 mM EGTA, 2 mM $MgCl_2$, 1% NP-40, 10% glycerol, 1 mM phenylmethylsulfonyl fluoride, 20 μg/ml aprotinin, and 2 mM DTT) for 15 min on ice. Lysates were clarified by centrifugation and incubated with agarose beads conjugated with the 9E10 anti-Myc antibody for 1 h at 4°C. The beads were then washed three times with immunoprecipitation buffer and finally resuspended in Laemmli's sample buffer. Proteins were resolved by SDS-PAGE for immunoblot analysis.

Immunofluorescence microscopy. Cells were grown on coverslips coated with poly-L-lysine and fixed with 3.7% formaldehyde for 10 min at room temperature. Fixed cells were then permeabilized with 0.1% Triton X-100 for 10 min. After being washed with phosphate-buffered saline, the cells were incubated with primary antibodies in phosphate-buffered saline containing 2% goat serum for 2 h, followed by incubation with Alexa Fluor-conjugated secondary antibodies (1:1,000 dilution; Invitrogen) for 1 h. F-actin was detected by staining with rhodamine-phalloidin or Alexa Fluor 647-conjugated phalloidin (Invitrogen). Samples were observed on an inverted microscope (model IX71; Olympus, Tokyo, Japan) equipped with a PlanApo 60×, 1.4-numerical-aperture (NA) oil immersion objective. Images were obtained with a cooled charge-coupled device camera (ORCA-ER; Hamamatsu Photonics, Shizuoka, Japan) controlled by Aqua-Lite software (Hamamatsu Photonics) and were processed using Adobe Photoshop CS3.

Boyden chamber assay. Cell migration was assayed in Boyden chambers (8.0-μm-pore-size polyethylene terephthalate membrane with Falcon cell culture insert; Becton Dickinson, Mountain View, CA) as previously described (7). NIH 3T3 cells transfected with EGFP, EPLINα-EGFP, or EPLINα(S360/602/692A)-EGFP were serum starved with DMEM containing 0.2% CS and then trypsinized and counted. Cells (5×10^4 to 10×10^4) in DMEM containing 0.2% CS (0.8 ml) were added to the upper chamber, and 1.8 ml of appropriate medium, with or without 30 ng/ml PDGF, was added to the lower chamber. When the MEK inhibitor was used in this assay, cells were treated with 20 μM U0126 for 30 min before trypsinization, and U0126 was also added to both the upper and lower chambers during migration. For RNAi rescue assays, cells were sequentially transfected with control siRNA or EPLIN siRNA and EGFP, EPLINαr-EGFP, or EPLINαr(S360/602/692A)-EGFP. For primary osteoblasts, α-minimum essential medium with 0.2% FBS was used. Transwells were incubated for 6 h at 37°C. EGFP-positive cells on both sides of the membrane were counted, and then cells on the inside of the insert were removed with a cotton swab and EGFP-positive

cells on the underside of the insert were counted. The number of cells in five randomly chosen fields per filter was counted by microscopic examination.

Live imaging. To observe PDGF-induced membrane ruffling, NIH 3T3 cells transfected with EPLINα-EGFP or EPLINα(S360/602/692A)-EGFP were stimulated with 50 ng/ml PDGF for 15 min after time-lapse recording. Time-lapse microscopy was performed using a DeltaVision deconvolution microscope system controlled by softWoRx software (Applied Precision, Issaquah, WA) configured around an Olympus IX70 inverted microscope. Images were acquired using a UPlanSApo 20×, 0.85-NA oil immersion objective. For wound-healing assays, after scratching of a monolayer of NIH 3T3 cells transfected with EPLINα-EGFP or EPLINα(S360/602/692A)-EGFP, live cells were recorded at 37°C in a 5% CO_2 atmosphere, using a confocal microscope (CSU22; Yokogawa, Tokyo, Japan) equipped with a cooled charge-coupled device camera (DV887DCS-BV; Andor Technology, Belfast, Northern Ireland). Images were acquired using a UPlanApo 20×, 0.80-NA oil immersion objective and were analyzed with MetaMorph software (Molecular Devices, Downingtown, PA).

RESULTS

ERK-mediated phosphorylation of EPLIN in living cells. To globally identify protein kinase substrates, we recently developed a system consisting of phosphoprotein purification by immobilized metal-affinity chromatography, fluorescent 2D-DIGE, and MS protein identification (20, 41). We applied this method to the ERK signaling pathway and identified 24 candidates for novel ERK targets, one of which was EPLIN (H. Kosako, N. Yamaguchi, M. Ushiyama, E. Nishida, and S. Hattori, submitted for publication).

To examine whether EPLIN is phosphorylated by ERK in living cells, Myc-tagged EPLIN was expressed in ΔB-Raf:ER cells. This cell line is a derivative of NIH 3T3 cells in which the protein kinase domain of mouse B-Raf is expressed as a fusion protein with the hormone-binding domain of the human estrogen receptor (32). ERK can be activated by 4-HT, an antagonist of estrogen. To suppress the ERK pathway, the MEK inhibitor U0126 was used. The lysates of these cells were subjected to immunoblotting with anti-Myc antibody (Fig. 1A, left panel). Both Myc-EPLINα and Myc-EPLINβ showed mobility shifts on SDS-PAGE upon treatment with 4-HT compared to treatment with U0126. To confirm phosphorylation as the cause of these shifts, we examined the effect of phosphatase treatment. Myc-EPLINβ was immunoprecipitated from 4-HT-treated ΔB-Raf:ER cells, and the immunoprecipitates were incubated with CIAP. As shown in Fig. 1A (right panel), the 4-HT-induced band shift of Myc-EPLINβ was completely reversed by CIAP treatment. These results suggest that EPLIN is phosphorylated by the activation of the ERK pathway. To determine the phosphorylation site on EPLIN that induces the mobility shift, HA-tagged wild-type EPLINβ and two Ser-to-Ala mutants were expressed in ΔB-Raf:ER cells, and then the cells were treated with 4-HT or U0126. HA-EPLINβ-S360A did not show the mobility shift (see Fig. S1 in the supplemental material), indicating that the shift was due to the phosphorylation of Ser360 (see below).

We generated a polyclonal antibody by immunizing a rabbit with bacterially expressed full-length mouse EPLINα fused to GST. To examine the specificity of the generated antibody, Flag-tagged EPLIN was expressed in NIH 3T3 cells. Both Flag-EPLINα and Flag-EPLINβ were detected by immunoblotting with our anti-EPLIN, commercially available anti-EPLIN (BL1141), and anti-Flag antibodies (Fig. 1B). The commercial anti-EPLIN (BL1141) antibody showed very little reactivity to endogenous EPLINα (Fig. 1B, middle panel). In contrast, our affinity-purified anti-EPLIN antibody specifically recognized endogenous EPLINα and also EPLINβ, as a faint band (Fig. 1B, left panel, and C). Since EPLINβ includes the entire sequence of EPLINα, EPLINβ is thought to be expressed at a much lower level than EPLINα in NIH 3T3 cells. When ΔB-Raf:ER cells were treated with 4-HT or when NIH 3T3 cells were stimulated with PDGF for 30 min, endogenous EPLINα and -β were phosphorylated, and this was prevented by pretreatment with U0126 (Fig. 1C).

ERK phosphorylates Ser360, Ser602, and Ser692 on EPLIN in vitro and in vivo. As described in the previous section, EPLIN is phosphorylated upon ERK activation. To test whether EPLIN is a direct substrate of ERK, we prepared GST fusion proteins of full-length EPLINα and the N-terminal and C-terminal portions of EPLINα, as illustrated schematically in Fig. 2A. An in vitro kinase assay was then performed, using recombinant active ERK, [γ-^{32}P]ATP, and recombinant GST-EPLINα, GST–EPLIN-N, and GST–EPLIN-C as substrates. Both GST-EPLINα and GST–EPLIN-C were strongly phosphorylated by ERK, whereas GST–EPLIN-N phosphorylation was rather weak (Fig. 2B, lanes 1, 3, and 6). It has been established that ERK preferentially phosphorylates Ser or Thr residues just before Pro residues (11). EPLIN has seven Ser-Pro sequences that are conserved between mouse and human EPLIN proteins (Fig. 2A). To identify ERK phosphorylation sites on EPLIN, we replaced each Ser residue with Ala. As shown in Fig. 2B, lane 4, the S360A substitution completely abolished ERK phosphorylation of EPLIN-N. On the other hand, replacement of either Ser602 or Ser692 by Ala partially abolished phosphorylation, and replacement of both residues (EPLIN-C-S602/692A) markedly reduced phosphorylation (Fig. 2B, lanes 9, 11, and 12). When full-length EPLINα was used as a substrate, replacement of Ser360, Ser602, and Ser692 by Ala (EPLINα-S360/602/692A) strongly impaired phosphorylation by ERK (Fig. 2B, lane 2). This suggests that Ser360, Ser602, and Ser692 are the primary sites at which ERK phosphorylates EPLIN in vitro.

To further confirm the phosphorylation sites, EPLIN phosphorylated by ERK in vitro was digested with trypsin or V8 protease, and the resulting peptides were subjected to LC-MS/MS analysis. As shown in Fig. S2 in the supplemental material, phosphorylation of Ser360, Ser602, and Ser692 was confirmed by this analysis. Phosphorylation of Ser488 and Ser607 was also observed, and these may be minor phosphorylation sites, as suggested by the slightly reduced phosphorylation of EPLIN-C-S488A and -S607A (Fig. 2B, lanes 8 and 10).

We then produced phospho-specific antibodies by using synthetic phosphopeptides that harbor phosphorylated Ser360, Ser602, or Ser692. The anti-pS360 antibody recognized wild-type GST–EPLIN-N and the S372A mutant of GST–EPLIN-N upon ERK-mediated phosphorylation but did not recognize the S360A mutant (Fig. 2C). Similarly, anti-pS602 and anti-pS692 antibodies recognized wild-type and S692A mutant GST-EPLIN-C and wild-type and S602A mutant GST–EPLIN-C, respectively, only when phosphorylated by ERK. These results indicate that the anti-pS360, anti-pS602, and anti-pS692 antibodies specifically recognize EPLIN phosphorylated at Ser360, Ser602, and Ser692, respectively.

To examine whether the anti-pS360, anti-pS602, and anti-

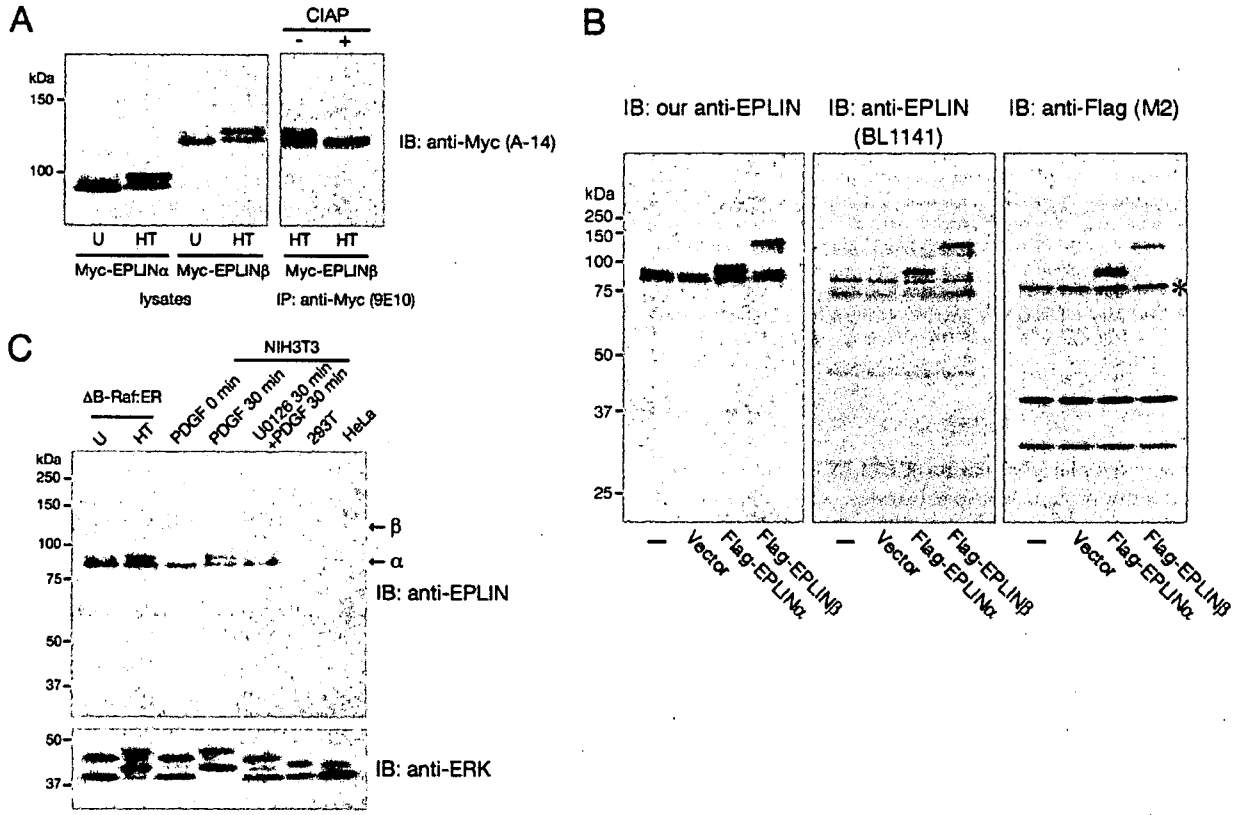

FIG. 1. ERK-mediated phosphorylation of EPLIN in living cells. (A) ΔB-Raf:ER cells transfected with Myc-EPLINα or -β were treated with 20 μM U0126 or 1 μM 4-HT for 2 h, and the lysates were immunoblotted with the A-14 anti-Myc rabbit antibody (left panel). Myc-EPLINβ-transfected cell lysates obtained for the left panel were immunoprecipitated with the 9E10 anti-Myc mouse antibody, and the immunoprecipitates were incubated with or without CIAP (right panel). (B and C) Our affinity-purified anti-mouse EPLIN antibody specifically recognized mouse but not human EPLIN. (B) NIH 3T3 cells were transfected with vector, Flag-EPLINα, or Flag-EPLINβ, as indicated, and immunoblotted with 0.25 μg/ml each of our anti-EPLIN, commercial anti-EPLIN (BL1141), and anti-Flag (M2) antibodies. All panel photos were taken at the same exposure time. The asterisk indicates nonspecific bands that migrated slightly faster than endogenous EPLINα. (C) ΔB-Raf:ER cells were treated with U0126 or 4-HT for 30 min, and serum-starved NIH 3T3 cells were stimulated with 50 ng/ml PDGF for 30 min in the presence or absence of a 30-min pretreatment with U0126. The lysates were immunoblotted with our anti-EPLIN and anti-ERK antibodies. EPLINβ bands became apparent after a longer exposure of the blot (data not shown).

pS692 antibodies can detect endogenous EPLIN phosphorylated by physiological stimuli that activate ERK, immunoblot analysis was performed on lysates from PDGF-stimulated NIH 3T3 cells. As shown in Fig. 2D, after the addition of PDGF, all three antibodies reacted with bands corresponding to EPLINα and EPLINβ. The time course of Ser602 and Ser692 phosphorylation was similar to that of ERK activation, but Ser360 phosphorylation proceeded slowly and increased for up to 240 min. Since the phosphorylation of Ser360 caused the mobility shift, anti-pS602 and anti-pS692 antibodies detected both EPLINα and -β as doublets at later time periods. When immunoblot analysis was performed on lysates from PDGF-stimulated primary calvarial osteoblasts, all three antibodies reacted with bands corresponding to EPLINα (see Fig. 10A). Phosphorylation of these three residues was strongly inhibited by pretreatment with U0126 (Fig. 2D; see Fig. 10A) or transfection with siRNA for ERK2 or ERK1 plus ERK2 (see Fig. 6A). Because the level of ERK2 expression in NIH 3T3 cells is significantly higher than that of ERK1 (note that comparable amounts of ERK1 and ERK2 bands were detected by immunoblotting with the K-23 anti-ERK1 antibody in all figures), it may be reasonable that phosphorylation of EPLIN as well as p90 ribosomal S6 kinase, a well-known ERK substrate, was not clearly inhibited by ERK1 depletion (see Fig. 6A). We therefore concluded that EPLIN is phosphorylated at Ser360, Ser602, and Ser692 by ERK in living cells.

Phosphorylation of the C-terminal region of EPLIN by ERK reduces its affinity for F-actin in vitro and in vivo. Because EPLIN has two actin-binding domains and cross-links actin filaments into bundles (23), we next examined whether phosphorylation of EPLIN regulates its association with F-actin. First, F-actin-binding properties of the nonphosphorylated and ERK-phosphorylated C-terminal region of EPLIN (GST–EPLIN-C) were compared by the F-actin cosedimentation assay in vitro (Fig. 3). In this assay, GST–EPLIN-C preincubated with or without ERK was mixed with purified actin filaments, the sample was ultracentrifuged, and the distribution of GST–EPLIN-C in the supernatant and pellet was examined. GST–EPLIN-C alone did not sediment, indicating that the sedimentation was due to binding to F-actin. The recovery of

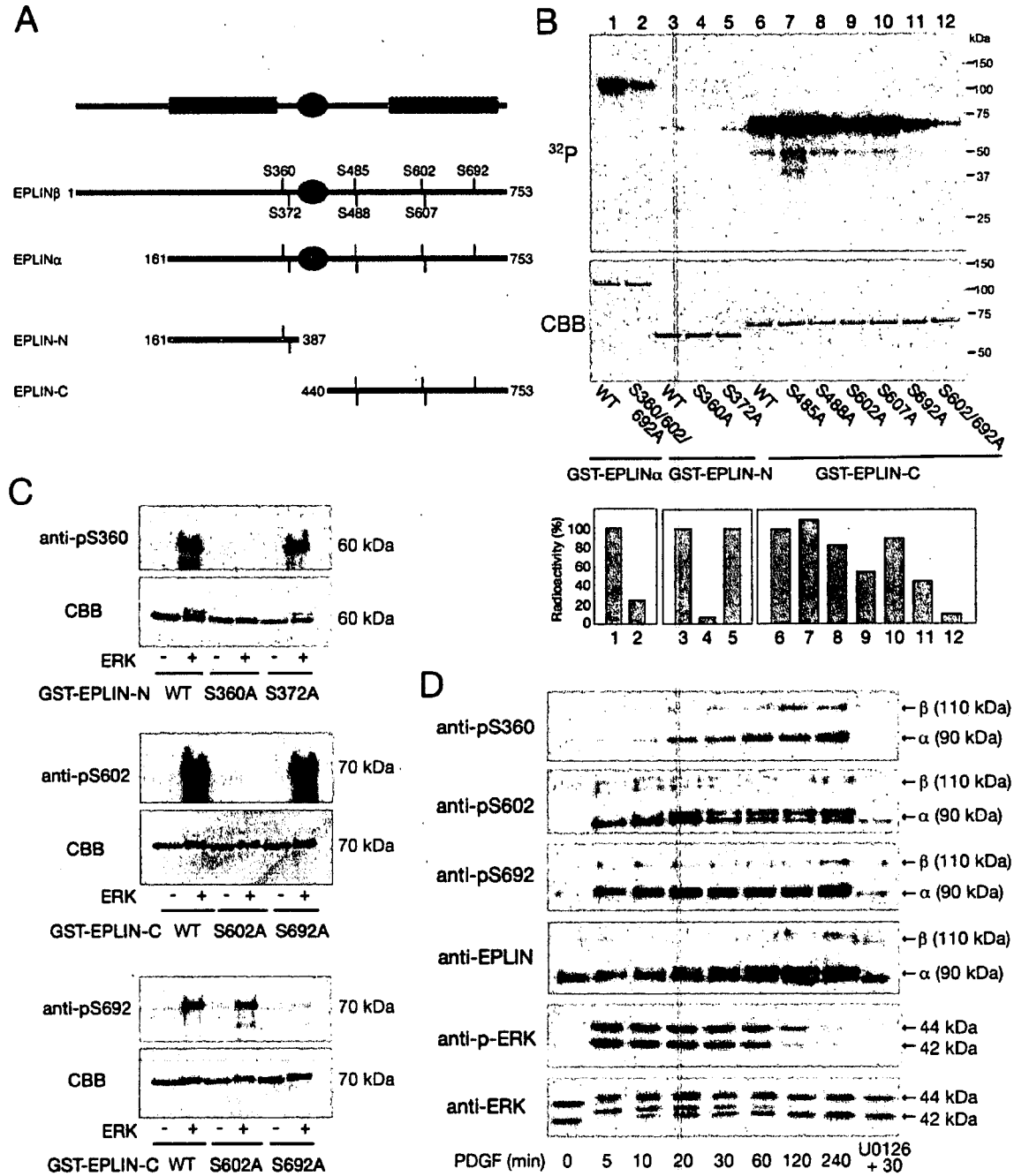

FIG. 2. ERK phosphorylates Ser360, Ser602, and Ser692 of EPLIN. (A) Domain structure of EPLIN and its truncation mutants. Potential ERK phosphorylation sites are indicated. For bacterial expression, EPLINα, EPLIN-N, and EPLIN-C were tagged with GST at the N terminus. (B) An in vitro kinase assay was performed using wild-type (WT) GST-EPLINα, GST–EPLIN-N, GST–EPLIN-C, and their Ser-to-Ala mutants as substrates and recombinant active ERK as a kinase in the presence of [γ-^{32}P]ATP. After electrophoresis, the gel was stained with CBB (middle panel) and subjected to autoradiography (upper panel). The relative intensities of phosphorylated bands were quantified by a Fujix BAS2000 bioimaging analyzer (lower panel). (C) GST–EPLIN-N, GST–EPLIN-C, and their Ala substitutes were incubated with or without ERK in vitro and analyzed by immunoblotting with anti-pS360, anti-pS602, and anti-pS692 antibodies as indicated. (D) Serum-starved NIH 3T3 cells treated with 10 ng/ml PDGF for the indicated times were analyzed by immunoblotting with the indicated antibodies.

ERK-phosphorylated wild-type GST–EPLIN-C in the pellet (35%) was significantly less than that of the nonphosphorylated form (59%), whereas the nonphosphorylatable mutant (S602/692A) of GST–EPLIN-C did not show ERK-dependent changes (63% recovery in the absence of ERK and 62% recovery in its presence) (Fig. 3A). To determine the stoichiometries of binding and dissociation constants (K_ds), various concentrations of these proteins were assayed for cosedimentation with a fixed amount of F-actin. As shown in Fig. 3B, the K_ds of nonphosphorylated and phosphorylated forms of wild-type

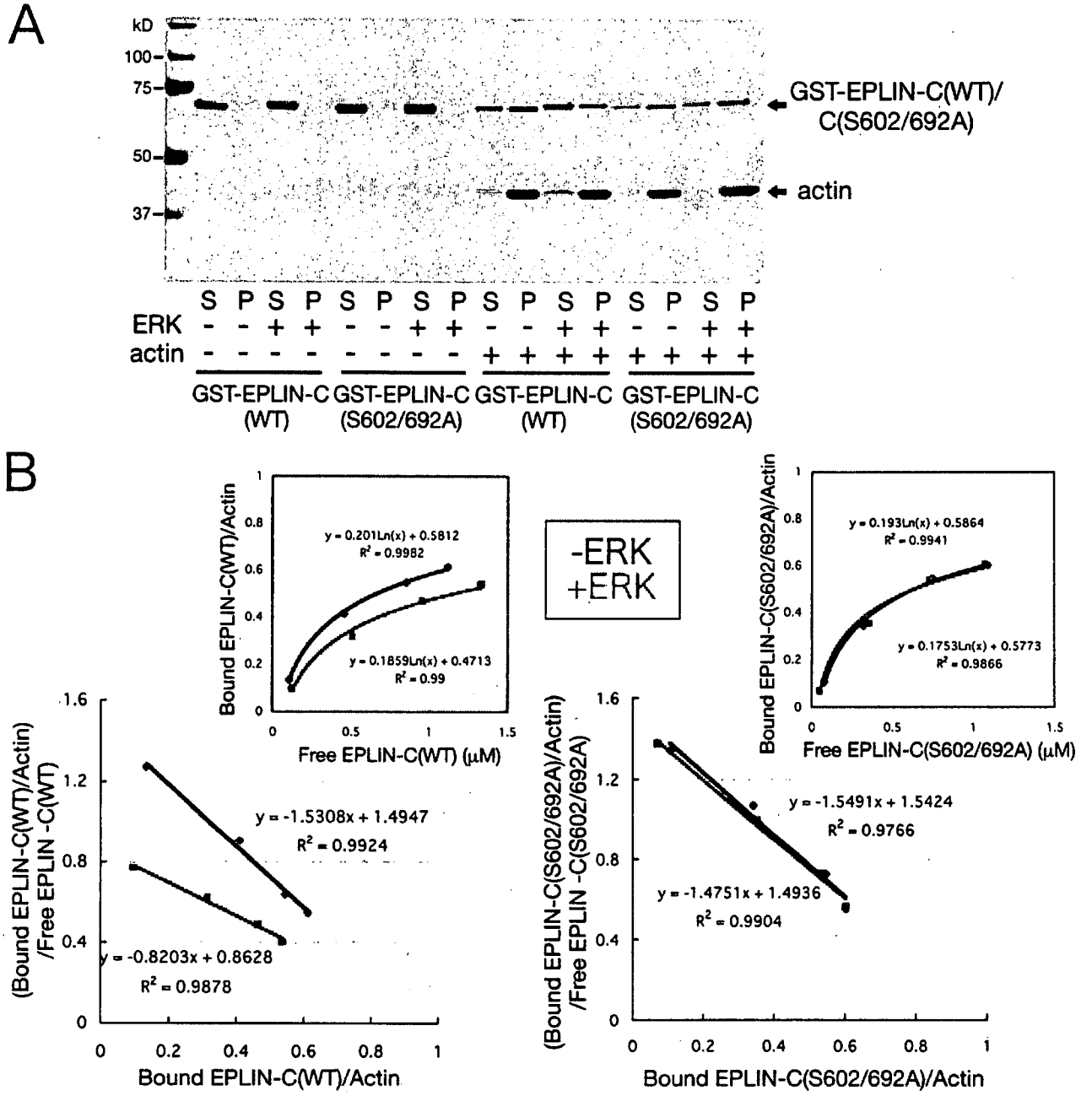

FIG. 3. Phosphorylation of the C-terminal region of EPLIN by ERK reduces its affinity for F-actin in vitro. (A) Phosphorylated (+ERK) or nonphosphorylated (−ERK) GST–EPLIN-C(WT) or GST–EPLIN-C(S602/692A) was mixed with (+) or without (−) 2.5 μM polymerized actin and ultracentrifuged. Supernatants (S) and pellets (P) were analyzed by SDS-PAGE followed by CBB staining. (B) Quantitative analysis of binding of the C-terminal region of EPLIN to actin filaments. The cosedimentation assay was performed by mixing 2.5 μM polymerized actin with various amounts of phosphorylated (red) or nonphosphorylated (black) GST–EPLIN-C(WT) (left panel) or GST–EPLIN-C(S602/692A) (right panel). Amounts of free and bound GST–EPLIN-C in the supernatant and pellet fractions were determined from a digitized CBB-stained gel.

GST–EPLIN-C for F-actin were calculated to be 0.65 μM and 1.2 μM, respectively. On the other hand, GST–EPLIN-C(S602/692A) preincubated with or without ERK showed similar binding properties for F-actin, with K_ds of ~0.6 μM. These results suggest that phosphorylation of the C-terminal region of EPLIN by ERK reduces its affinity for F-actin. In contrast, phosphorylation of full-length EPLIN and the N-terminal region of EPLIN by ERK did not significantly reduce their affinity for F-actin in a similar in vitro actin cosedimentation assay (data not shown).

To test the effect of ERK phosphorylation of EPLIN on its affinity for actin in vivo, Myc-tagged full-length EPLIN or the

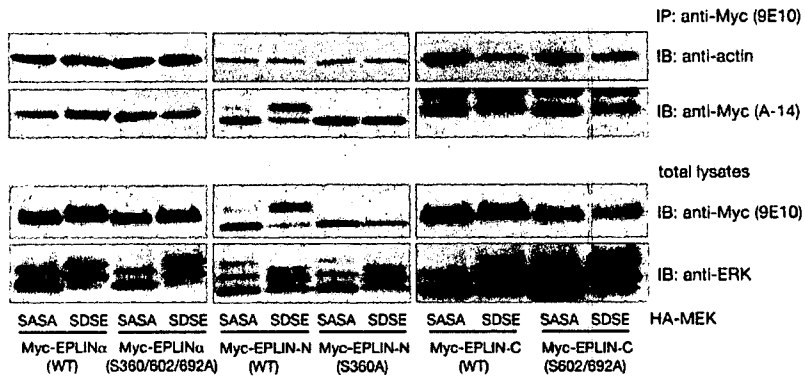

FIG. 4. Phosphorylation of the C-terminal region of EPLIN by ERK reduces its affinity for actin in vivo. 293T cells were cotransfected with Myc-EPLINα, Myc–EPLIN-N, Myc–EPLIN-C, or their Ala substitutes and dominant-negative (SASA) or constitutively active (SDSE) HA-MEK as indicated. The lysates were immunoprecipitated with an anti-Myc (9E10) antibody, followed by immunoblot analysis with antiactin and anti-Myc (A-14) antibodies (upper panels). The total lysates were immunoblotted with anti-Myc (9E10) and anti-ERK antibodies (lower panels).

N-terminal or C-terminal region of EPLIN was coexpressed with constitutively active (SDSE) or dominant-negative (SASA) HA-tagged MEK in 293T cells. Myc-EPLIN was immunoprecipitated with anti-Myc antibody, and immunoprecipitates were subjected to immunoblotting with anti-actin (Fig. 4). The coexpression of MEK-SDSE markedly decreased the binding of EPLIN-C to actin compared to coexpression of MEK-SASA, while the binding of EPLIN-C(S602/692A) did not change upon ERK activation (Fig. 4, right panels). Full-length Myc-EPLINα and Myc–EPLIN-N did not show such a reduction (Fig. 4, left and middle panels). EPLIN may homodimerize through a LIM domain and bind to the side of an actin filament through two actin-binding domains (23). Therefore, it may be reasonable that a reduction in the actin-binding activity of the C-terminal region does not necessarily result in a significant decrease in that of full-length EPLIN (see Fig. 9F).

Stimulation with PDGF induces relocalization of EPLIN to peripheral and dorsal ruffles. To examine whether phosphorylation by ERK regulates EPLIN function in living cells, we first investigated the subcellular localization of EPLIN during ERK activation. Serum-starved NIH 3T3 cells were stimulated with PDGF and then immunostained with anti-EPLIN (Fig. 5A). EPLIN colocalized with actin stress fibers in quiescent cells (Fig. 5A, left panels). PDGF stimulation induced disassembly of stress fibers and formation of peripheral and dorsal ruffles, where EPLIN was relocalized (Fig. 5A, middle panels). When cells were treated with PDGF in the presence of U0126, stress fiber disassembly was partially inhibited, and a fraction of EPLIN localized on the remaining stress fibers (Fig. 5A, right panels). Similar results were obtained with primary osteoblasts (see Fig. 10B).

Stimulation with PDGF induces phosphorylation of Ser360 and Ser602 at peripheral and dorsal ruffles. We then examined the localization of phosphorylated EPLIN in PDGF-stimulated NIH 3T3 cells by indirect immunofluorescence microscopy using anti-pS360 and anti-pS602 antibodies (Fig. 5B and C; the anti-pS692 antibody did not show specific staining). In quiescent cells, phosphorylation of Ser360 was hardly detected. When cells were stimulated with PDGF, Ser360-phosphorylated EPLIN appeared first in peripheral and dorsal ruffles and gradually increased with time (Fig. 5B), consistent with the results of immunoblot analysis (Fig. 2D). U0126 pretreatment or siRNA-mediated depletion of ERK2 or ERK1 plus ERK2 completely abolished the staining by the anti-Ser360 antibody (Fig. 5B and 6B).

Immunostaining with the anti-pS602 antibody revealed that phosphorylation of EPLIN at Ser602 proceeded earlier than that at Ser360 (Fig. 5C). After 5 min of stimulation with PDGF, phosphorylation signals clearly appeared in dorsal ruffles (Fig. 5C, arrowheads). The time course of anti-pS602 staining intensity also correlated well with the results of immunoblot analysis. Phosphorylated ERK (p-ERK) was observed throughout the cell body after 5 min, translocated into the nucleus after 30 min, and returned to the cytoplasm after 120 min (Fig. 5C). These staining patterns with anti-pS602 and anti-p-ERK antibodies were abolished by U0126 pretreatment or siRNA-mediated depletion of ERK2 or ERK1 plus ERK2 (Fig. 5C and 6B and C). Nuclear staining with the anti-pS602 antibody was observed in quiescent cells and in cells pretreated with U0126, suggesting that it may be nonspecific staining.

Ser360- and Ser602-phosphorylated EPLIN localizes to the leading edge of migrating cells. The localization of phosphorylated EPLIN at membrane ruffles prompted us to test whether the phosphorylation of EPLIN occurs during cell migration. Wound healing of fibroblasts causes a rapid and transient activation of ERK at the leading edge, which can be inhibited by U0126 (21, 26). Six hours after wounding of a confluent monolayer of NIH 3T3 cells, cells were immunostained with the anti-pS360 or anti-pS602 antibody (Fig. 7). Both phosphorylated Ser360 and Ser602 were evident in cells at the leading edge. As expected, pretreatment with U0126 completely abolished these staining patterns. These results indicate that EPLIN is phosphorylated by ERK at the leading edge of migrating fibroblasts.

Phosphorylation of EPLIN by ERK is required for PDGF-induced stress fiber disassembly and membrane ruffling. To examine whether the phosphorylation of EPLIN by ERK is involved in membrane ruffling, we constructed EGFP-fused full-length EPLINα (EPLINα-EGFP) and a nonphosphorylatable mutant EPLINα protein [EPLINα(S360/602/692A)-EGFP] in which three major phosphorylation sites were re-

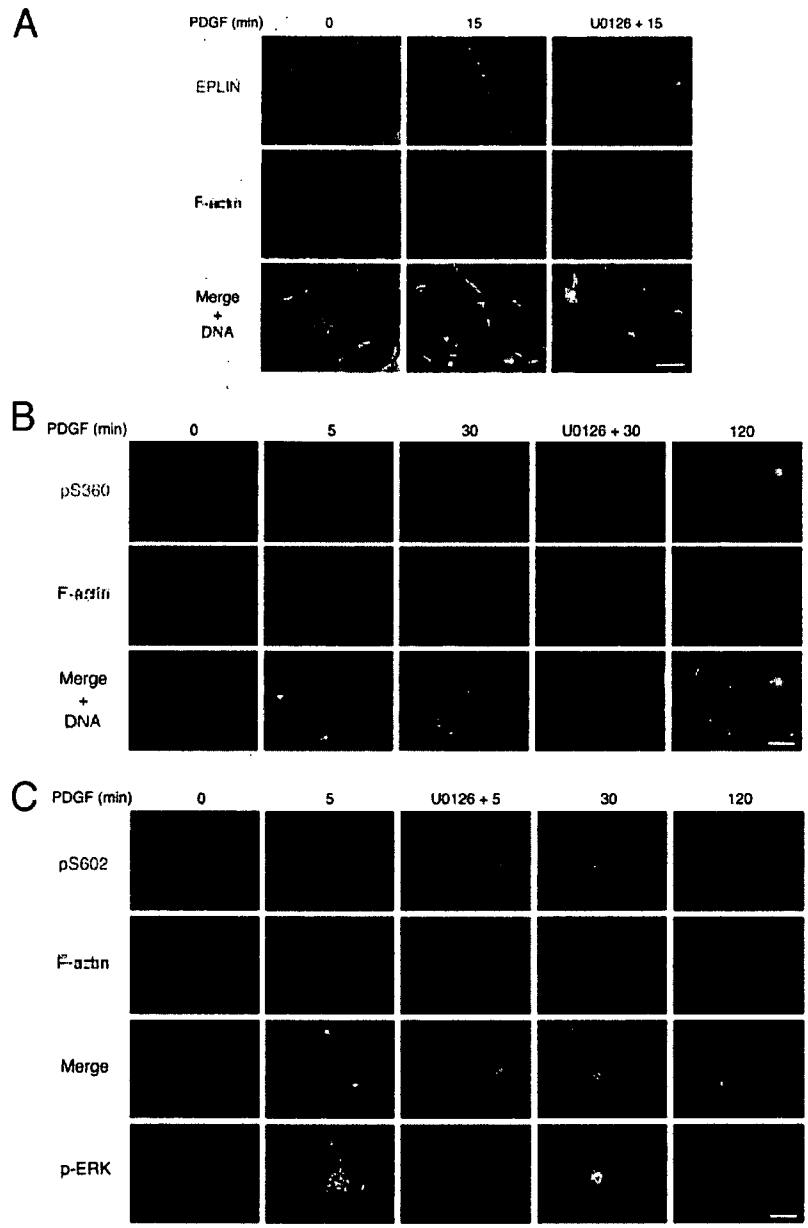

FIG. 5. Stimulation with PDGF induces localization of phosphorylated EPLIN to peripheral and dorsal ruffles. Serum-starved NIH 3T3 cells were stimulated with 50 ng/ml PDGF for the indicated times in the presence or absence of a 30-min pretreatment with U0126. (A) Cells were fixed and stained with the anti-EPLIN antibody (green), rhodamine-phalloidin (red), and DAPI (4′,6′-diamidino-2-phenylindole) (blue). (B) Cells were fixed and stained with the anti-pS360 antibody (green), rhodamine-phalloidin (red), and DAPI (blue). (C) Cells were fixed and stained with the anti-pS602 antibody (green), Alexa Fluor 647-phalloidin (red), and anti-p-ERK antibody (gray). Note that Ser602-phosphorylated EPLIN preferentially localizes to membrane ruffles rather than stress fibers. The arrows and arrowheads indicate peripheral and dorsal ruffles, respectively. Bars, 30 μm.

placed with Ala. Expression of both types of EPLIN increased the number and size of actin stress fibers in quiescent NIH 3T3 cells (Fig. 8A, left panels), as reported previously for MCF-7 cells (23). After stimulation with PDGF, EPLINα-EGFP-expressing cells lost their stress fibers and formed prominent lamellipodia/membrane ruffles, but EPLINα(S360/602/692A)-EGFP-expressing cells still retained stress fibers and formed fewer membrane ruffles (Fig. 8A, right panels; see Videos S1 and S2 in the supplemental material).

EGPF-positive cells were categorized into four classes according to their degree of ruffling (Fig. 8B). Among quiescent cells, most wild type- and Ala mutant-transfected cells were classified as type I (without ruffles). When cells were stimulated with PDGF for 5 min, EPLINα-EGFP-expressing cells were mostly classified into types III and IV, with marked lamellipodia/membrane ruffles, but in EPLINα(S360/602/692A)-EGFP-expressing cells ruffle formation was significantly impaired. These data suggest that phosphorylation of EPLIN by

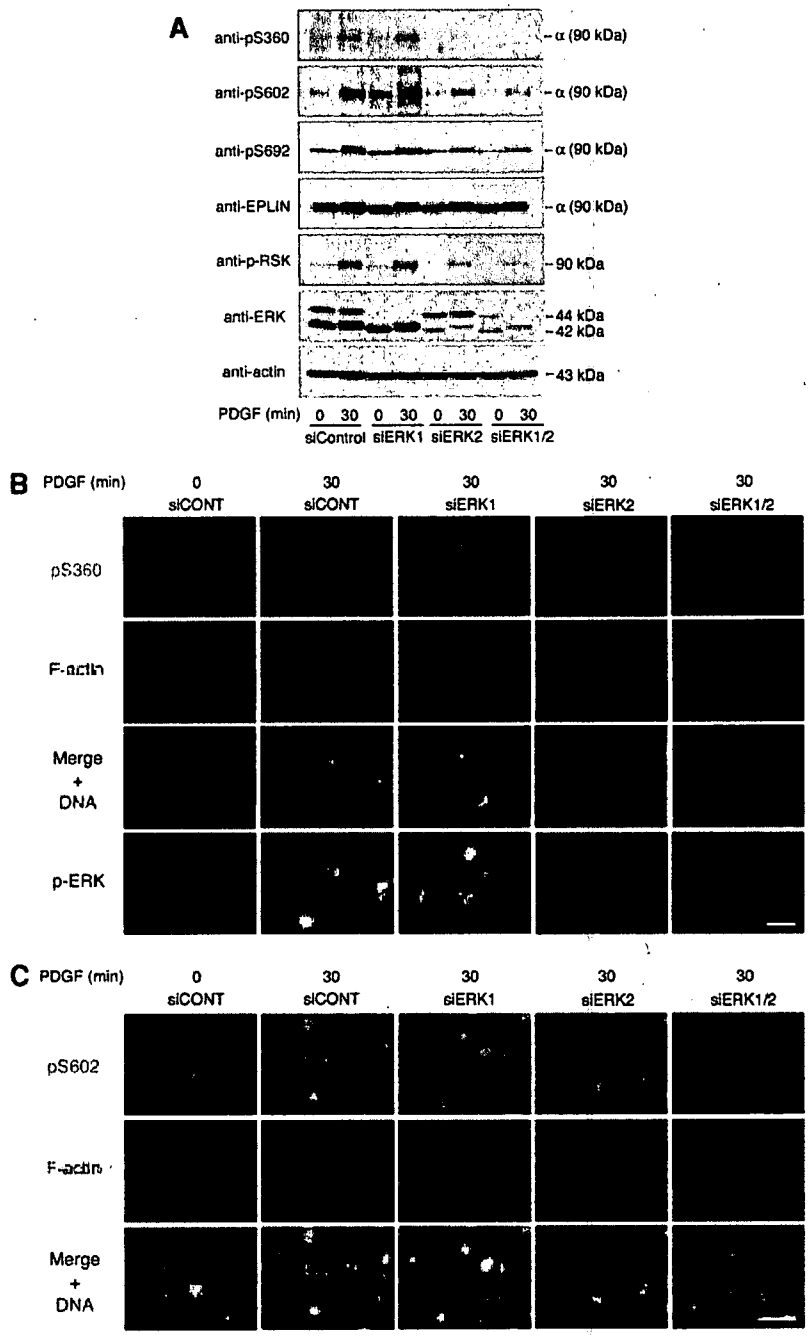

FIG. 6. PDGF-induced phosphorylation of EPLIN is inhibited by siRNA-mediated depletion of ERK2 or ERK1 plus ERK2. NIH 3T3 cells were transfected with siRNA for control, ERK1, ERK2, or ERK1 plus ERK2, incubated for 48 h, serum starved, and then stimulated with 50 ng/ml PDGF for 0 or 30 min. (A) The lysates were immunoblotted with the indicated antibodies. (B) Cells were fixed and quadruply stained with the anti-pS360 antibody (green), Alexa Fluor 647-phalloidin (red), DAPI (blue), and anti-p-ERK antibody (gray). (C) Cells were fixed and triply stained with the anti-pS602 antibody (green), rhodamine-phalloidin (red), and DAPI (blue). Bars, 30 μm.

ERK is involved in PDGF-induced lamellipodium/membrane ruffle formation.

Phosphorylation of EPLIN by ERK is required for cell migration. Dynamic phosphorylation and dephosphorylation of cytoskeletal proteins are essential for effective cell motility. To evaluate the potential role of EPLIN phosphorylation in cell migration, wound-healing assays were performed using EPLINα-EGFP- and EPLINα(S360/602/692A)-EGFP-transfected NIH 3T3 cells. The proportion of EGFP-positive cells at the wound edge was assessed over an 8-h time period. The ratio of EPLINα-EGFP expression at the wound edge (approximately 20%) did not change during

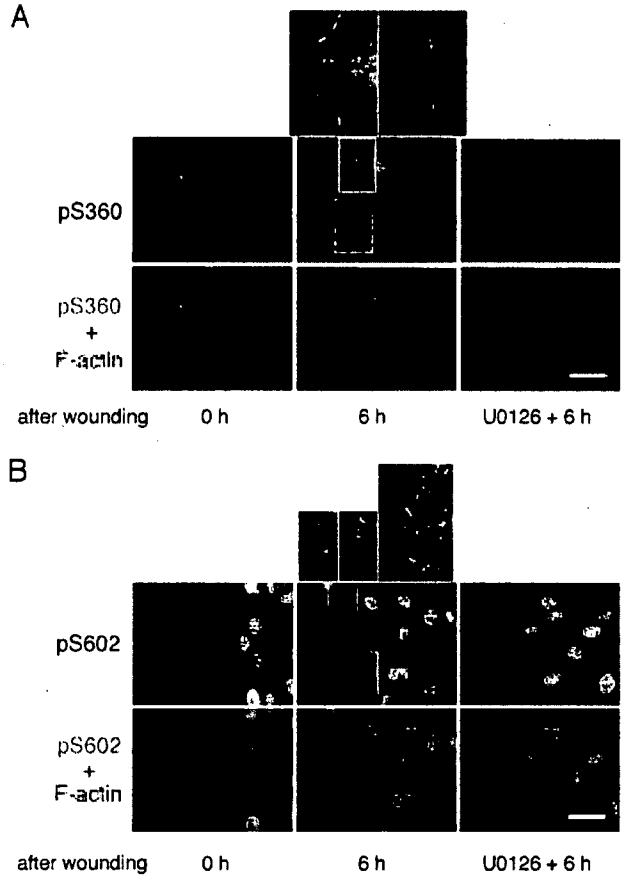

FIG. 7. EPLIN is phosphorylated at the leading edge of migrating fibroblasts during recovery from a wound. A confluent monolayer of NIH 3T3 cells was "wounded" by being scraped with a plastic pipette tip and then cultured for 0 or 6 h in the presence or absence of a 30-min pretreatment with U0126. Cells were fixed and doubly stained with the anti-pS360 (A) or anti-pS602 (B) antibody and rhodamine-phalloidin (red). The wound site is at the left of each panel. Bars, 50 μm.

this period, indicating that EPLINα-EGFP-expressing cells and surrounding untransfected cells migrated at similar velocities (Fig. 9A; see Video S3 in the supplemental material). In contrast, the EPLINα(S360/602/692A)-EGFP-expressing cells showed a marked decrease in motility and gradually fell behind the wound edge during recovery (Fig. 9A; see Video S4 in the supplemental material). These results indicate that EPLIN phosphorylation by ERK is required for cell migration during wound healing.

The roles of EPLIN phosphorylation by ERK in cell motility were evaluated in another experiment, a modified Boyden chamber assay. The addition of PDGF to the lower chamber induced migration of NIH 3T3 cells expressing EGFP or EPLINα-EGFP, and pretreatment with U0126 inhibited PDGF-induced migration of these cells (Fig. 9B). In contrast, expression of EPLINα(S360/602/692A)-EGFP significantly inhibited PDGF-induced migration compared with expression of EGFP or EPLINα-EGFP (Fig. 9B). Similar results were obtained with primary osteoblasts (Fig. 10C). These results suggest that EPLIN phosphorylation by ERK is also required for PDGF-induced cell migration.

To further investigate the functions of EPLIN in cell motility, siRNA-mediated depletion of EPLIN and rescue assays were performed. We prepared RNAi-refractory versions of EPLIN proteins [EPLINαr-EGFP and EPLINαr(S360/602/692A)-EGFP] harboring silent mutations (Fig. 9C). EPLIN depletion significantly enhanced the ability of NIH 3T3 cells to migrate in both the wound-healing assay and the modified Boyden chamber assay (Fig. 9D and E), suggesting that EPLIN functions to negatively influence cell motility. While expression of EPLINαr-EGFP efficiently restored the enhanced migratory activity to the level seen with control siRNA treatment, EPLINαr(S360/602/692A)-EGFP-expressing cells showed a significant decrease in motility compared with control siRNA-treated or EPLINαr-EGFP-expressing cells (Fig. 9D and E). We also confirmed these findings by performing modified Boyden chamber assays with primary osteoblasts (Fig. 10D). Taken together, these results indicate that EPLIN phosphorylation by ERK is required for cell migration.

DISCUSSION

In the present study, we have characterized an F-actin cross-linking protein, EPLIN, as a novel ERK MAPK substrate. First, ERK phosphorylates EPLIN on Ser360, Ser602, and Ser692 in vitro and in living cells. Second, ERK phosphorylation of EPLIN decreases the affinity of its C-terminal region for actin filaments. Third, EPLIN localizes to actin stress fibers in quiescent cells, and stimulation with PDGF induces relocalization of EPLIN to lamellipodia/membrane ruffles. Fourth, phosphorylated EPLIN localizes to membrane ruffles both upon PDGF stimulation and during wound healing. Fifth, a non-ERK-phosphorylatable mutant of EPLIN inhibits PDGF-dependent actin stress fiber disassembly, membrane ruffling, and cell migration, while RNAi-mediated silencing of EPLIN enhances cell motility. ERK thus controls actin organization and cell motility by phosphorylating EPLIN.

ERK phosphorylation sites within EPLIN were identified by site-directed mutagenesis. We determined that the Ser360, Ser602, and Ser692 residues of EPLIN are the major phosphorylation sites for ERK. These phosphorylation sites were confirmed by LC-MS/MS analysis of in vitro-phosphorylated EPLIN (see Fig. S2A, C, and D in the supplemental material). Immunoblot analysis using phospho-specific antibodies revealed that these three sites are indeed phosphorylated by ERK in intact cells (Fig. 2D and 10A). Although recent phosphoproteomic studies detected intracellular phosphorylation of mouse EPLIN at Ser360 (43) and of human EPLIN at Ser604 and Ser698 (corresponding to Ser602 and Ser692 of mouse EPLIN) (27, 28), spatiotemporal changes had not been reported. Interestingly, PDGF-induced phosphorylation of Ser360 occurred rather slowly compared to the rapid phosphorylation of Ser602, Ser692, and ERK (Fig. 2D). This raises the possibility that cellular phosphatase activity toward Ser360 is high in the early phase or that ERK indirectly phosphorylates Ser360 through a downstream kinase.

EPLIN contains two actin-binding sites, in the N- and C-terminal halves, and a LIM domain between these sites may allow EPLIN to homodimerize. EPLIN therefore cross-links

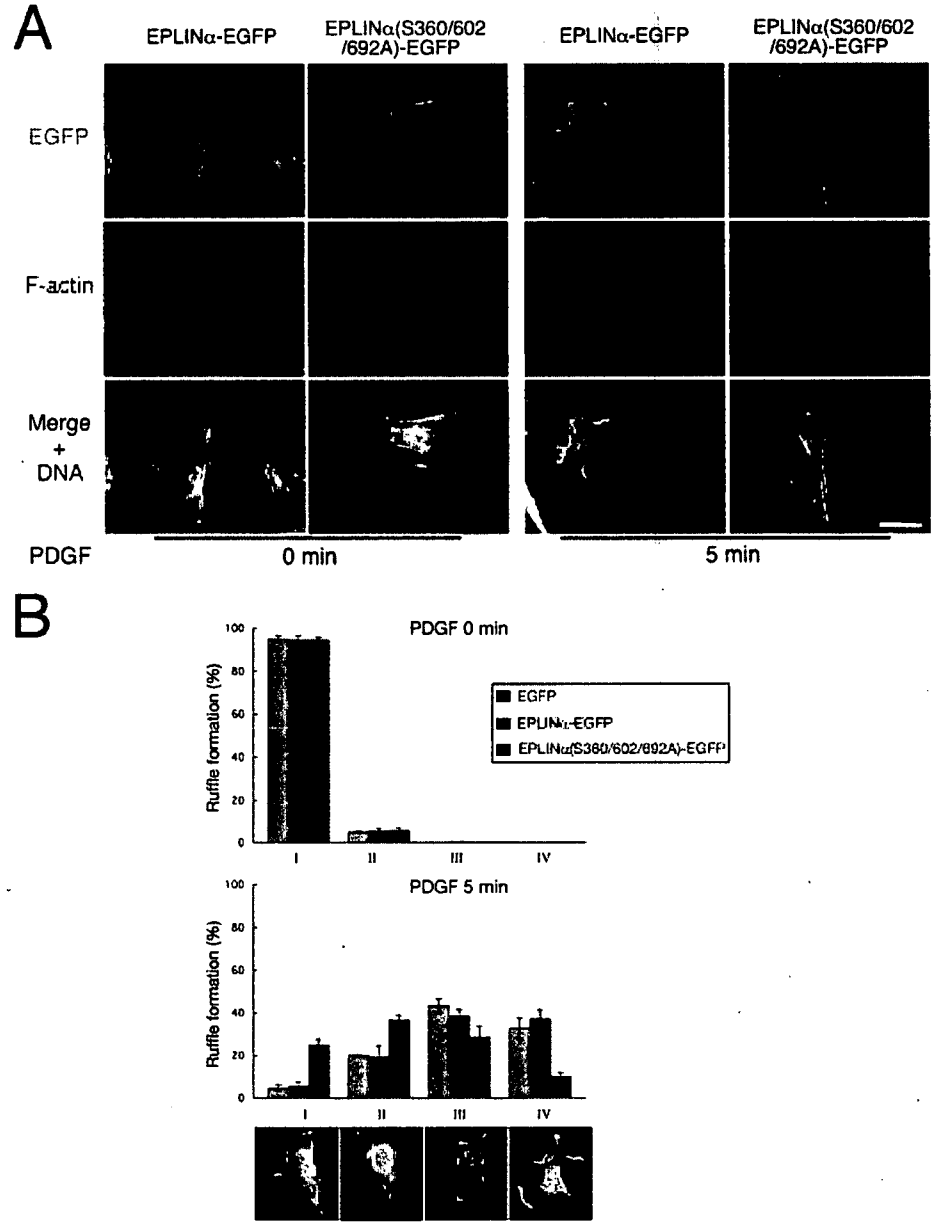

FIG. 8. Phosphorylation of EPLIN is required for PDGF-induced stress fiber disassembly and membrane ruffling. (A) NIH 3T3 cells transfected with EPLINα-EGFP or EPLINα(S360/602/692A)-EGFP were stimulated with 50 ng/ml PDGF for 0 or 5 min. Cells were fixed and stained with rhodamine-phalloidin and DAPI to detect F-actin (red) and DNA (blue), respectively. Bar, 30 μm. (B) NIH 3T3 cells transfected with EGFP, EPLINα-EGFP, or EPLINα(S360/602/692A)-EGFP were stimulated with 50 ng/ml PDGF for 0 or 5 min. The degree of ruffling was categorized into four classes, as exemplified in the bottom panels. At least 100 cells were counted per sample, and values are means ± standard deviations (SD) for three independent experiments.

and bundles actin filaments, but the two actin-binding domains may have different functions in the cell (23). In cosedimentation assays with F-actin, we found that the C-terminal half of EPLIN, but neither full-length EPLIN nor the N-terminal half of EPLIN, reduces its association with F-actin upon ERK-mediated phosphorylation. This observation was confirmed by an in vivo experiment showing that the amount of actin coimmunoprecipitated with the C-terminal half but neither full-length EPLIN nor the N-terminal half of EPLIN was reduced by activation of ERK. Since EPLIN is supposed to bind to the side of an actin filament through two actin-binding domains (23), it may be reasonable that a reduction in the actin-binding activity of the C-terminal region does not necessarily lead to a significant decrease in that of full-length EPLIN (Fig. 9F).

The phosphorylation-dependent reduction of the affinity of the C-terminal region for F-actin may affect the actin-bundling activity of EPLIN to facilitate dynamic remodeling of actin filament networks. Thus, we investigated the effects of EPLIN

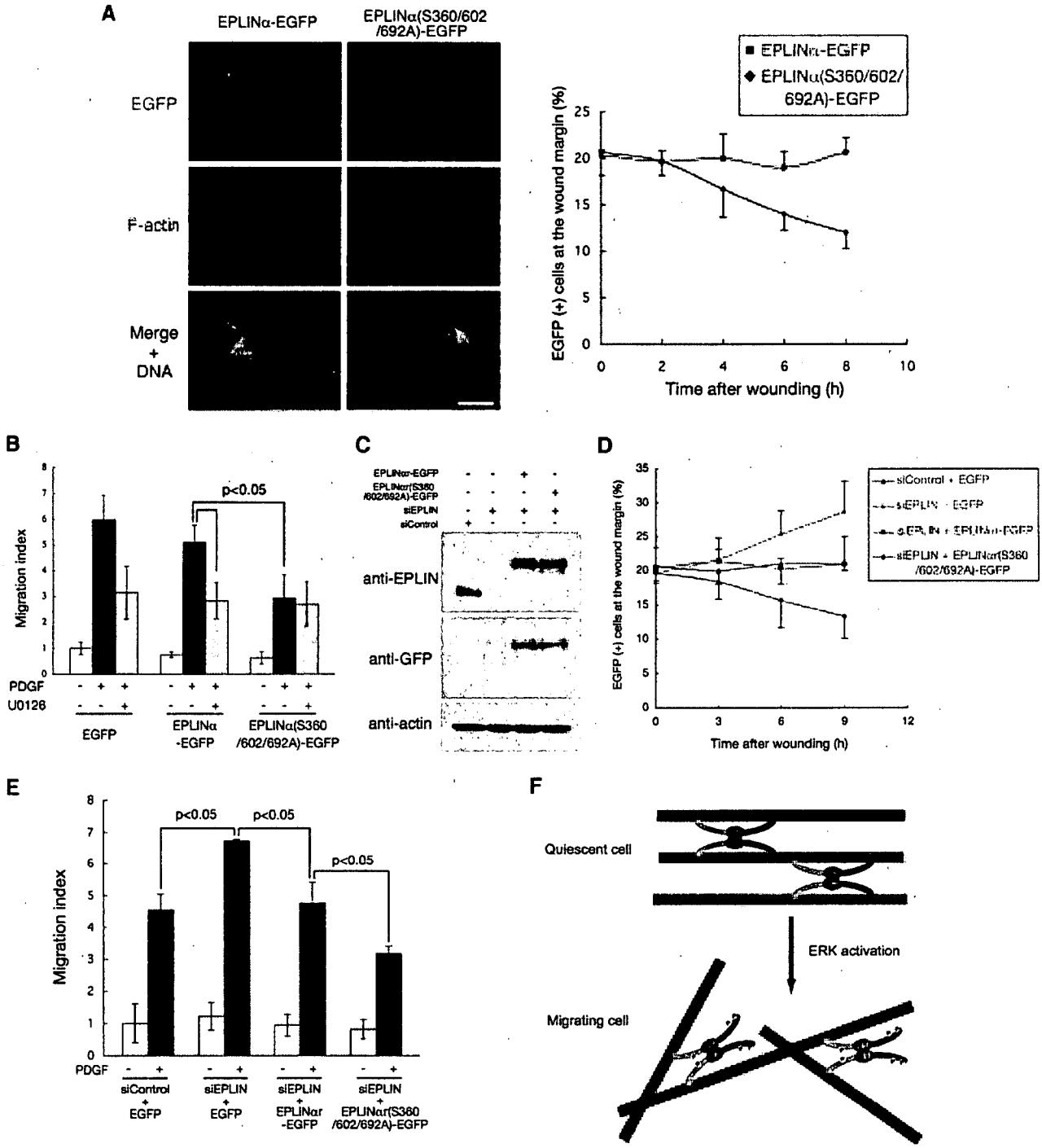

FIG. 9. Phosphorylation of EPLIN is required for cell migration. (A) Six hours after wounding of a confluent monolayer of NIH 3T3 cells transfected with EPLINα-EGFP or EPLINα(S360/602/692A)-EGFP, cells were fixed and stained with rhodamine-phalloidin and DAPI to detect F-actin (red) and DNA (blue), respectively (left panels; both EGFP-positive cells were located at the margin immediately after being wounded). The wound site is at the left of each panel. Bar, 50 μm. At the indicated times after wounding, the proportion of EGFP-positive cells at the wound margin was assessed (right panel). (B) NIH 3T3 cells were transfected with EGFP, EPLINα-EGFP, or EPLINα(S360/602/692A)-EGFP. After 24 h, a modified Boyden chamber assay was performed in the absence or presence of 30 ng/ml PDGF in the lower chamber. PDGF-induced migration was also observed in the presence of 20 μM U0126 in both the upper and lower chambers. (C) NIH 3T3 cells were transfected with control siRNA or EPLIN siRNA, incubated for 24 h, and then transfected with EGFP, RNAi-refractory EPLINαr-EGFP, or EPLINαr(S360/602/692A)-EGFP. After 24 h of incubation, the lysates were immunoblotted with the indicated antibodies. (D) At the indicated times after being wounded, a confluent monolayer of NIH 3T3 cells that had been transfected simultaneously as indicated were fixed and stained as described for panel A, and the proportion of EGFP-positive cells at the wound margin was assessed. (E) NIH 3T3 cells were sequentially transfected as described for panel C and then subjected to a modified Boyden chamber assay in the absence or presence of 30 ng/ml PDGF in the lower chamber. For panels A, B, D, and E, at least 100 cells were counted per sample, and values are means ± SD for three independent experiments. (F) Schematic representation of the proposed mechanism by which ERK-mediated phosphorylation of the C-terminal region of EPLIN leads to reorganization of actin filaments.

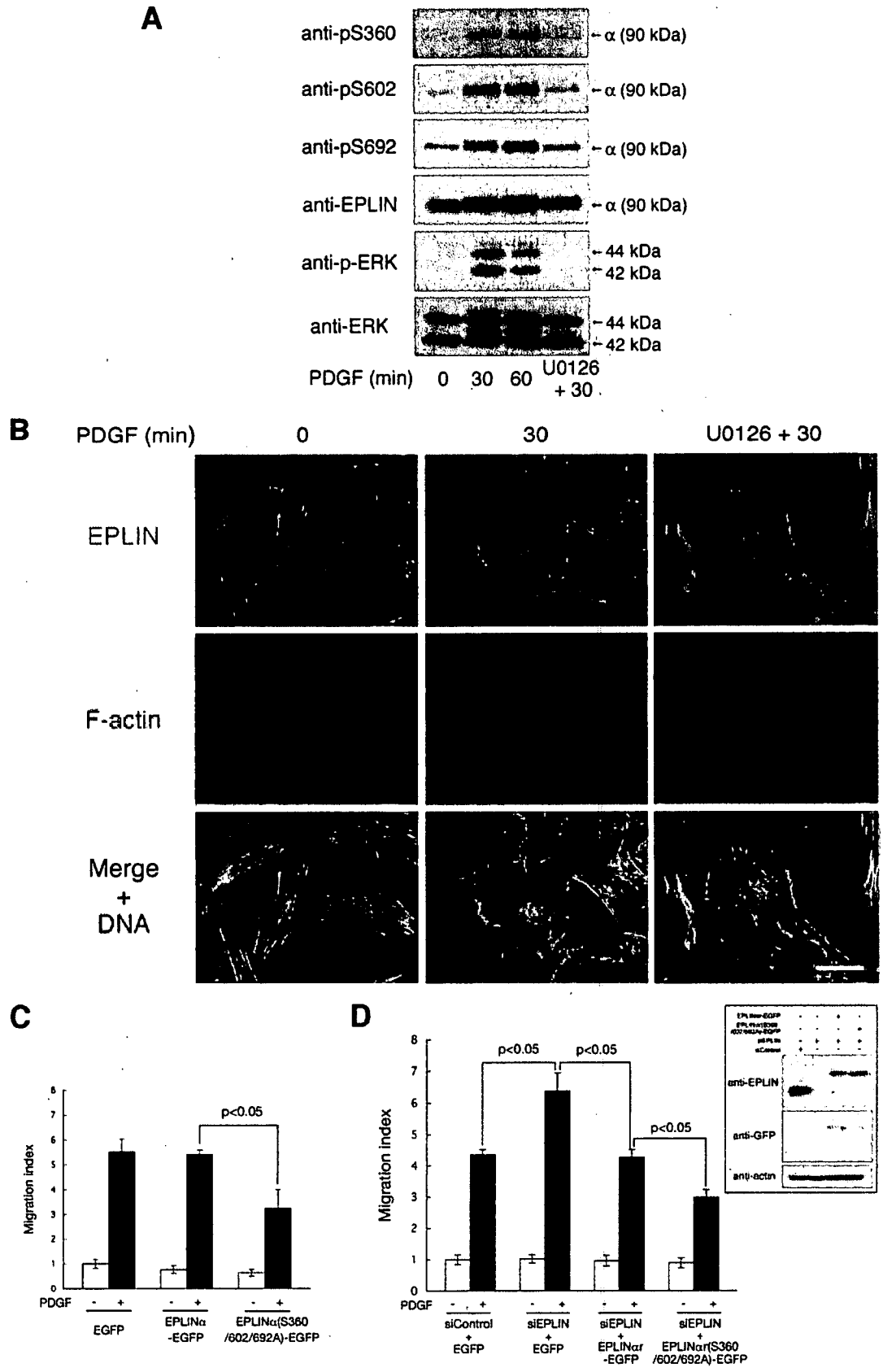

phosphorylation on its localization, actin dynamics, and cell motility. It has been reported that endogenous EPLIN is distributed predominantly along actin stress fibers in U2OS cells (35). Consistent with this finding, immunostaining showed that EPLIN colocalized with stress fibers in quiescent NIH 3T3 cells (Fig. 5A) and primary osteoblasts (Fig. 10B). Stimulation with PDGF induced stress fiber disassembly and relocalization of EPLIN to membrane ruffles within 15 to 30 min. When cells were treated with PDGF in the presence of U0126, stress fiber disassembly was partly inhibited by blocking the ERK pathway (29), and a fraction of EPLIN remained localized on the resultant stress fibers.

We further demonstrated by indirect immunofluorescence microscopy that both Ser360 and Ser602 are phosphorylated in specific subcellular areas by PDGF stimulation or during cell migration, suggesting the physiological significance of these phosphorylation sites in cellular processes. Both staining patterns were not detectable when the cells were pretreated with U0126 (Fig. 5B and C and Fig. 7) or transfected with siRNA for ERK2 or ERK1 plus ERK2 (Fig. 6B and C), indicating ERK-dependent phosphorylation. PDGF treatment induced the phosphorylation of EPLIN at peripheral and dorsal ruffles. In migrating NIH 3T3 fibroblasts, phosphorylated EPLIN preferentially localized to the leading edge, which is consistent with previous observations that activated ERK is also localized at the leading edge during migration of rat embryo fibroblasts and 3Y1 cells (21, 26). These findings support the possible involvement of EPLIN phosphorylation by ERK in actin reorganization and cell migration (see below).

To clarify the effects of EPLIN phosphorylation on actin organization and cell motility, we used wild-type EPLIN and a non-ERK-phosphorylatable mutant EPLINα fused to EGFP. The nonphosphorylatable mutant inhibited both cellular processes. The precise molecular mechanism by which ERK promotes ruffle formation and cell migration via phosphorylating EPLIN remains unclear. Since the mutant contains substitutions in both the N- and C-terminal regions, there remained the possibility that the reduction of the affinity of the C-terminal region for F-actin may not participate in this mechanism. However, in a modified Boyden chamber assay, two substitutions in the C-terminal region [EPLINα(S602/692A)-EGFP migration index, 3.53 ± 0.46] showed a similar inhibitory effect to that by three substitutions [EPLINα(S360/602/692A)-EGFP migration index, 3.03 ± 0.35] compared with the wild type (EPLINα-EGFP migration index, 5.17 ± 0.47) or a protein with one substitution in the N-terminal region [EPLINα(S360A)-EGFP migration index, 4.67 ± 0.52], indicating the importance of a phosphorylation-dependent reduction in the C-terminal binding activity. Phosphorylation of Ser360 in the N-terminal region causes an electrophoretic mobility shift (see Fig. S1 in the supplemental material), suggesting conformational and functional changes that should be addressed in future studies. Since nonphosphorylated EPLIN dimers can form thick actin bundles through the N- and C-terminal actin-binding sites, EPLIN in quiescent cells may stabilize stress fibers and inhibit cell migration (Fig. 9F, upper panel). Phosphorylated EPLIN dimers can cross-link actin filaments through only the N-terminal actin-binding sites, and thereby EPLIN in migrating cells may form a dynamic actin meshwork in membrane ruffles (Fig. 9F, lower panel). Taken together, the data show that PDGF stimulation activates ERK, which phosphorylates EPLIN to reduce the affinity of its C-terminal region for actin filaments, and then phosphorylated EPLIN causes destabilization of stress fibers and reorganization of the actin cytoskeleton to form membrane ruffles and to enhance cell migration.

ERK is known to regulate actin organization and cell motility by phosphorylating a number of proteins, including MLCK, FAK, paxillin, actopaxin, and vinexin. We demonstrate in this study that EPLIN is also a mediator of ERK-regulated cytoskeletal dynamics. Because the expression of phosphomimetic mutants of EPLIN had weak effects on these processes (data not shown), many actin-binding proteins phosphorylated by ERK are likely to act in concert to regulate actin dynamics. Furthermore, various extracellular stimuli induce actin reorganization and cell migration through other ERK-independent pathways. For example, it was recently reported that Akt regulates these processes via phosphorylation of girdin, an F-actin cross-linking protein (7). Other actin cross-linking proteins, such as fascin (42, 45) and L-plastin (15), were also shown to be regulated by phosphorylation to control actin cytoskeletal assembly and cell motility.

It has been reported that EPLIN is down-regulated or lost in a number of oral, prostate, and breast cancer cell lines (3, 22). Since siRNA-mediated depletion of EPLIN enhanced cell motility during wound healing and in PDGF-induced cell migration, the down-regulation of EPLIN expression might be relevant to migration and invasion of these cancer cells. Previously, it was reported that ectopic expression of EPLIN can suppress anchorage-independent growth of NIH 3T3 cells transformed by Cdc42V12 or EWS/Fli-1 but not by RasV12 (35). This can now be explained by actin reorganization and enhanced cell motility through the Ras-Raf-MEK-ERK-EPLIN pathway. Ras-mediated phosphorylation of EPLIN may be involved in the invasion of tumor cells with Ras mutations. EPLIN is highly conserved from zebra fish to humans and contains multiple Ser/Thr-Pro motifs that can potentially be phosphorylated by ERK. The ERK-EPLIN pathway may play important roles in diverse physiological processes in vertebrates.

FIG. 10. Phosphorylation of EPLIN by ERK is required for cell migration in primary calvarial osteoblasts. (A and B) Serum-starved osteoblasts were treated with 50 ng/ml PDGF for the indicated times in the presence or absence of a 30-min pretreatment with U0126. (A) The lysates were immunoblotted with the indicated antibodies. (B) Cells were fixed and stained with the anti-EPLIN antibody (green), rhodamine-phalloidin (red), and DAPI (blue). Bar, 30 μm. (C) Osteoblasts were transfected with EGFP, EPLINα-EGFP, or EPLINα(S360/602/692A)-EGFP. After 24 h, a modified Boyden chamber assay was performed in the absence or presence of 30 ng/ml PDGF in the lower chamber. (D) Osteoblasts sequentially transfected with control siRNA or EPLIN siRNA and EGFP, EPLINαr-EGFP, or EPLINαr(S360/602/692A)-EGFP were subjected to a modified Boyden chamber assay in the absence or presence of 30 ng/ml PDGF in the lower chamber. The inset shows the depletion of endogenous EPLINα by siRNA and the rescue by RNAi-refractory EPLINαr-EGFP or EPLINαr(S360/602/692A)-EGFP. For panels C and D, at least 100 cells were counted per sample, and values are means ± SD for three independent experiments.

ACKNOWLEDGMENTS

We thank Michimoto Kobayashi for his help during the initial stages of this work, Yutaka Harita for help with rabbit immunization, Makoto Watanabe for help with isolating primary calvarial osteoblasts, Hiroyuki Fukuda for LC-MS/MS analysis, Miho Ohsugi and Noriko Tokai-Nishizumi for help with time-lapse video microscopy, Masanori Mishima and Max Douglas for critical readings of the manuscript, and Shiro Suetsugu and Eisuke Nishida for helpful discussions and advice. We also thank Martin McMahon for kindly providing ΔB-Raf:ER cells.

This work was supported in part by grants-in-aid for scientific research from the Japan Society for the Promotion of Science (to H.K.) and the Encouraging Development Strategic Research Centers Program, Special Coordination Funds for Promoting Science and Technology, the Ministry of Education, Culture, Sports, Science, and Technology (to S.H.). This work was also supported by grants from the Nakajima Foundation (to H.K.) and the Novartis Foundation (Japan) for the Promotion of Science (to S.H.). This work was developed and coordinated under the framework of the program for the International Research and Educational Institute for Integrated Medical Sciences (IREIIMS).

REFERENCES

1. **Adams, J. C.** 2004. Roles of fascin in cell adhesion and motility. Curr. Opin. Cell Biol. **16**:590–596.
2. **Bartles, J. R.** 2000. Parallel actin bundles and their multiple actin-bundling proteins. Curr. Opin. Cell Biol. **12**:72–78.
3. **Chang, D. D., N. H. Park, C. T. Denny, S. F. Nelson, and M. Pe.** 1998. Characterization of transformation related genes in oral cancer cells. Oncogene **16**:1921–1930.
4. **Chang, L., and M. Karin.** 2001. Mammalian MAP kinase signalling cascades. Nature **410**:37–40.
5. **Clarke, D. M., M. C. Brown, D. P. LaLonde, and C. E. Turner.** 2004. Phosphorylation of actopaxin regulates cell spreading and migration. J. Cell Biol. **166**:901–912.
6. **Cox, B. D., M. Natarajan, M. R. Stettner, and C. L. Gladson.** 2006. New concepts regarding focal adhesion kinase promotion of cell migration and proliferation. J. Cell Biochem. **99**:35–52.
7. **Enomoto, A., H. Murakami, N. Asai, N. Morone, T. Watanabe, K. Kawai, Y. Murakumo, J. Usukura, K. Kaibuchi, and M. Takahashi.** 2005. Akt/PKB regulates actin organization and cell motility via Girdin/APE. Dev. Cell **9**:389–402.
8. **Etienne-Manneville, S., and A. Hall.** 2002. Rho GTPases in cell biology. Nature **420**:629–635.
9. **Fincham, V. J., M. James, M. C. Frame, and S. J. Winder.** 2000. Active ERK/MAP kinase is targeted to newly forming cell-matrix adhesions by integrin engagement and v-Src. EMBO J. **19**:2911–2923.
10. **Glading, A., R. J. Bodnar, I. J. Reynolds, H. Shiraha, L. Satish, D. A. Potter, H. C. Blair, and A. Wells.** 2004. Epidermal growth factor activates m-calpain (calpain II), at least in part, by extracellular signal-regulated kinase-mediated phosphorylation. Mol. Cell. Biol. **24**:2499–2512.
11. **Gonzalez, F. A., D. L. Raden, and R. J. Davis.** 1991. Identification of substrate recognition determinants for human Erk1 and Erk2 protein kinases. J. Biol. Chem. **266**:22159–22163.
12. **Hazzalin, C. A., and L. C. Mahadevan.** 2002. MAPK-regulated transcription: a continuously variable gene switch? Nat. Rev. Mol. Cell. Biol. **3**:30–40.
13. **Huang, C., K. Jacobson, and M. D. Schaller.** 2004. MAP kinases and cell migration. J. Cell Sci. **117**:4619–4628.
14. **Hunger-Glaser, I., E. P. Salazar, J. Sinnett-Smith, and E. Rozengurt.** 2003. Bombesin, lysophosphatidic acid, and epidermal growth factor rapidly stimulate focal adhesion kinase phosphorylation at Ser-910: requirement for ERK activation. J. Biol. Chem. **278**:22631–22643.
15. **Janji, B., A. Giganti, V. De Corte, M. Catillon, E. Bruyneel, D. Lentz, J. Plastino, J. Gettemans, and E. Friederich.** 2006. Phosphorylation on Ser5 increases the F-actin-binding activity of L-plastin and promotes its targeting to sites of actin assembly in cells. J. Cell Sci. **119**:1947–1960.
16. **Klemke, R. L., S. Cai, A. L. Giannini, P. J. Gallagher, P. de Lanerolle, and D. A. Cheresh.** 1997. Regulation of cell motility by mitogen activated protein kinase. J. Cell Biol. **137**:481–492.
17. **Kondoh, K., S. Torii, and E. Nishida.** 2005. Control of MAP kinase signaling to the nucleus. Chromosoma **114**:86–91.
18. **Lewis, T. S., P. S. Shapiro, and N. G. Ahn.** 1998. Signal transduction through MAP kinase cascades. Adv. Cancer Res. **74**:49–139.
19. **Liu, Z. X., C. F. Yu, C. Nickel, S. Thomas, and L. G. Cantley.** 2002. Hepatocyte growth factor induces ERK-dependent paxillin phosphorylation and regulates paxillin-focal adhesion kinase association. J. Biol. Chem. **277**:10452–10458.
20. **Machida, M., H. Kosako, K. Shirakabe, M. Kobayashi, M. Ushiyama, J. Inagawa, J. Hirano, T. Nakano, Y. Bando, E. Nishida, and S. Hattori.** 2007. Purification of phosphoproteins by immobilized metal affinity chromatography and its application to phosphoproteome analysis. FEBS J. **274**:1576–1587.
21. **Matsubayashi, Y., M. Ebisuya, S. Honjoh, and E. Nishida.** 2004. ERK activation propagates in epithelial cell sheets and regulates their migration during wound healing. Curr. Biol. **14**:731–735.
22. **Maul, R. S., and D. D. Chang.** 1999. EPLIN, epithelial protein lost in neoplasm. Oncogene **18**:7838–7841.
23. **Maul, R. S., Y. Song, K. J. Amann, S. C. Gerbin, T. D. Pollard, and D. D. Chang.** 2003. EPLIN regulates actin dynamics by cross-linking and stabilizing filaments. J. Cell Biol. **160**:399–407.
24. **Mitsushima, M., A. Suwa, T. Amachi, K. Ueda, and N. Kioka.** 2004. Extracellular signal-regulated kinase activated by epidermal growth factor and cell adhesion interacts with and phosphorylates vinexin. J. Biol. Chem. **279**: 34570–34577.
25. **Nguyen, D. H., A. D. Catling, D. J. Webb, M. Sankovic, L. A. Walker, A. V. Somlyo, M. J. Weber, and S. L. Gonias.** 1999. Myosin light chain kinase functions downstream of Ras/ERK to promote migration of urokinase-type plasminogen activator-stimulated cells in an integrin-selective manner. J. Cell Biol. **146**:149–164.
26. **Nobes, C. D., and A. Hall.** 1999. Rho GTPases control polarity, protrusion, and adhesion during cell movement. J. Cell Biol. **144**:1235–1244.
27. **Nousiainen, M., H. H. W. Silljé, G. Sauer, E. A. Nigg, and R. Körner.** 2006. Phosphoproteome analysis of the human mitotic spindle. Proc. Natl. Acad. Sci. USA **103**:5391–5396.
28. **Olsen, J. V., B. Blagoev, F. Gnad, B. Macek, C. Kumar, P. Mortensen, and M. Mann.** 2006. Global, in vivo, and site-specific phosphorylation dynamics in signaling networks. Cell **127**:635–648.
29. **Orr, A. W., M. A. Pallero, and J. E. Murphy-Ullrich.** 2002. Thrombospondin stimulates focal adhesion disassembly through Gi- and phosphoinositide 3-kinase-dependent ERK activation. J. Biol. Chem. **277**:20453–20460.
30. **Pearson, G., F. Robinson, T. B. Gibson, B. E. Xu, M. Karandikar, K. Berman, and M. H. Cobb.** 2001. Mitogen-activated protein (MAP) kinase pathways: regulation and physiological functions. Endocr. Rev. **22**:153–183.
31. **Pollard, T. D., and G. G. Borisy.** 2003. Cellular motility driven by assembly and disassembly of actin filaments. Cell **112**:453–465.
32. **Pritchard, C. A., M. L. Samuels, E. Bosch, and M. McMahon.** 1995. Conditionally oncogenic forms of the A-Raf and B-Raf protein kinases display different biological and biochemical properties in NIH 3T3 cells. Mol. Cell. Biol. **15**:6430–6442.
33. **Revenu, C., R. Athman, S. Robine, and D. Louvard.** 2004. The co-workers of actin filaments: from cell structures to signals. Nat. Rev. Mol. Cell. Biol. **5**:635–646.
34. **Ridley, A. J.** 2001. Rho GTPases and cell migration. J. Cell Sci. **114**:2713–2722.
35. **Song, Y., R. S. Maul, C. S. Gerbin, and D. D. Chang.** 2002. Inhibition of anchorage-independent growth of transformed NIH3T3 cells by epithelial protein lost in neoplasm (EPLIN) requires localization of EPLIN to actin cytoskeleton. Mol. Biol. Cell **13**:1408–1416.
36. **Stambolic, V., and J. R. Woodgett.** 2006. Functional distinctions of protein kinase B/Akt isoforms defined by their influence on cell migration. Trends Cell Biol. **16**:461–466.
37. **Stossel, T. P., J. Condeelis, L. Cooley, J. H. Hartwig, A. Noegel, M. Schleicher, and S. S. Shapiro.** 2001. Filamins as integrators of cell mechanics and signaling. Nat. Rev. Mol. Cell. Biol. **2**:138–145.
38. **Stupack, D. G., S. Y. Cho, and R. L. Klemke.** 2000. Molecular signaling mechanisms of cell migration and invasion. Immunol. Res. **21**:83–88.
39. **Suetsugu, S., and T. Takenawa.** 2007. Stress-associated MAP kinase fills in the map of filamin-mediated neuronal migration. Dev. Cell **12**:3–4.
40. **Tomar, A., Y. Wang, N. Kumar, S. George, B. Ceacareanu, A. Hassid, K. E. Chapman, A. M. Aryal, C. M. Waters, and S. Khurana.** 2004. Regulation of cell motility by tyrosine phosphorylated villin. Mol. Biol. Cell **15**:4807–4817.
41. **Ueda, K., H. Kosako, Y. Fukui, and S. Hattori.** 2004. Proteomic identification of Bcl2-associated athanogene 2 as a novel MAPK-activated protein kinase 2 substrate. J. Biol. Chem. **279**:41815–41821.
42. **Vignjevic, D., S. Kojima, Y. Aratyn, O. Danciu, T. Svitkina, and G. G. Borisy.** 2006. Role of fascin in filopodia protrusion. J. Cell Biol. **174**:863–875.
43. **Villén, J., S. A. Beausoleil, S. A. Gerber, and S. P. Gygi.** 2007. Large-scale phosphorylation analysis of mouse liver. Proc. Natl. Acad. Sci. USA **104**: 1488–1493.
44. **Waskiewicz, A. J., and J. A. Cooper.** 1995. Mitogen and stress response pathways: MAP kinase cascades and phosphatase regulation in mammals and yeast. Curr. Opin. Cell Biol. **7**:798–805.
45. **Yamakita, Y., S. Ono, F. Matsumura, and S. Yamashiro.** 1996. Phosphorylation of human fascin inhibits its actin binding and bundling activities. J. Biol. Chem. **271**:12632–12638.
46. **Zhang, Z., S. Y. Lin, B. G. Neel, and B. Haimovich.** 2006. Phosphorylated α-actinin and protein-tyrosine phosphatase 1B coregulate the disassembly of the focal adhesion kinase × Src complex and promote cell migration. J. Biol. Chem. **281**:1746–1754.